Anuário do Instituto de Geociências
Universidade Federal do Rio de Janeiro
https://revistas.ufrj.br/index.php/aigeo/

ISSN 0101-9759
e-ISSN 1982-3908

GEOLOGY

Poços de Caldas – Cabo Frio Alignment: a Petrochronological Review of an Unconventional Plume Model

Alinhamento Poços de Caldas – Cabo Frio: uma Revisão Petrocronológica de um Modelo de Pluma Não Convencional

Marco Aurélio Maia Teodoro[1], Anderson Costa dos Santos[1], Luiz Carlos Bertolino[1], Pedro Augusto da Silva Rosa[2], Caio Rodrigues Bezerra[3], Lucas Guimarães Pereira Monteiro[1], Júlio César Lopes da Silva[4], Mariana Bessa Fagundes[2], Mauro Cesar Geraldes[2], Leticia Muniz da Costa Cardoso[2] & Fred Jourdan[5]

[1] Universidade do Estado do Rio de Janeiro, Faculdade de Geologia, Departamento de Mineralogia e Petrologia Ígnea, Rio de Janeiro, RJ, Brasil
[2] Universidade Federal de Minas Gerais, Instituto de Geociências, Departamento de Geologia, Belo Horizonte, MG, Brasil
[3] Universidade Federal de Roraima, Instituto de Geociências, Boa Vista, RR, Brasil
[4] Universidade Federal do Rio de Janeiro, Departamento de Geologia, Rio de Janeiro, RJ, Brasil
[5] Curtin University, School of Earth and Planetary Sciences and John de Laeter Centre, Western Australian Argon Isotope Facility, Perth, Western Australia, Australia

E-mails: marcomaia.geo@hotmail.com; andcostasantos@gmail.com; lcbertolino@uol.com.br; pedro.rosa.geo@gmail.com; caiogeoufrr@gmail.com; lucasgpmonteiro@gmail.com; jlopes@geologia.ufrj.br; marianafbessa@gmail.com; maurogeraldes@gmail.com; leticiamuniz_@hotmail.com; f.jourdan@exchange.curtin.edu.au

Abstract

This work reviews the Poços de Caldas – Cabo Frio Alignment (PCCFA), one of Brazil's alkaline igneous provinces, comprising syenites, phonolites, and trachytes, as well as magmatic breccias. TAS and Harker (for major and trace elements) diagrams suggest two groups based on the silica content. From the TAS diagram, it is noted that the less evolved rocks plot mainly in the tephrite/basanite and foidite fields, while the more evolved rocks predominantly fall in the phonolite and trachyte fields. In the Harker diagrams, correlations with silica can be observed for some oxides/elements, such as TiO_2, CaO, Rb, Sr, Zr, Y, and Nb. From the normalized diagrams, it is evident that the less evolved rocks exhibit low variability, indicating similar sources and petrogenetic processes. In contrast, the more evolved ones present several anomalies (Ba, Sr, Ti, Rb, Zr, and Eu), suggesting different mineral fractionations. In addition, a wide range of normalized values is observed for certain elements, such as Ba, Sr, and Pb, which may indicate distinct evolutionary processes. Sr and Nd isotopic data show show similar trends, suggesting a mixture of DMM and EMI or DMM and EMII sources for the PCCFA complexes. Two new $^{40}Ar/^{39}Ar$ ages (71.55 ± 0.49 Ma and 67.31 ± 0.78 Ma) are presented for the Tinguá and Itatiaia massifs, respectively. In addition, two new U-Pb ages (69.3 ± 2.2 Ma for Tinguá and 70.4 ± 2.6 Ma for Itatiaia) are presented along with a third U-Pb age of 65 ± 2 Ma obtained for Gatos Hill, which is the first published age for this massif. The compilation of geochronological data, along with these new ages, indicates that the decrease in ages from west to east is not regular. For example, the oldest age (Itatiaia – 90.5 Ma) and the youngest age (Tinguá – 39.1 Ma) are found in more central massifs of the magmatic alignment. This feature prevents the genesis of this alignment from being attributed to a conventional plume model. In this regard, the authors suggest the presence of a plume with widespread conduits that have used preexisting structures for the intrusion the alkaline rocks, a hypothesis supported by the orientation of these magmatic bodys (massifs and dikes).

Keywords: Alkaline Province; $^{40}Ar/^{39}Ar$ dating; U-Pb dating

Received: August 21, 2024; Accepted: November 2, 2024

Resumo

Este trabalho estuda o Alinhamento Poços de Caldas – Cabo Frio (APCCF), uma das províncias ígneas alcalinas do Brasil, que é composta por diferentes tipos de sienitos, fonolitos e traquitos, além de brechas magmáticas. Os diagramas TAS e de Harker (maiores e traços) sugerem dois grupos com base no conteúdo de sílica. A partir do primeiro diagrama nota-se que as rochas menos evoluídas plotam principalmente nos campos tefrito/basanito e foidito, enquanto as mais evoluídas caem principalmente nos campos fonolito e traquito. Nos diagramas Harker correlações com sílica podem ser verificadas para alguns óxidos/elementos, como TiO_2, CaO, Rb, Sr, Zr, Y e Nb. A partir dos diagramas normalizados verifica-se que as rochas menos evoluídas apresentam baixa variabilidade, indicando fontes e processos petrogenéticos semelhantes. Já as rochas mais evoluídas apresentam diversas anomalias (como Ba, Sr, Ti, Rb, Zr e Eu), sugerindo diferentes fracionamentos minerais. Além disso, nota-se um range grande de valores normalizados para alguns elementos, como Ba, Sr e Pb, o que pode indicar processos evolutivos distintos. Os dados isotópicos de Sr e Nd mostram comportamentos semelhantes, sugerindo mistura de fontes de DMM e EMI ou DMM e EMII para os complexos APCCF. São apresentadas duas novas idades de $^{40}Ar/^{39}Ar$ de 71,55 ± 0,49 Ma e 67,31 ± 0,78 Ma para os maciços Tinguá e Itatiaia, respectivamente. Além disso, duas novas idades U-Pb de 69,3 ± 2,2 Ma (Tinguá) e 70,4 ± 2,6 Ma (Itatiaia) são apresentadas, além de uma terceira idade U-Pb de 65 ± 2 Ma obtida para o Maciço Morro dos Gatos, a qual é a primeira idade publicada. A compilação de dados geocronológicos, além destas novas idades, indica que a diminuição das idades de oeste para leste não é regular pois, por exemplo, as idades mais velha (Itatiaia – 90.5 Ma) e mais nova (Tinguá – 39.1 Ma) encontram-se em maciços mais centrais do alinhamento magmático. Tal característica impede que a gênese deste alinhamento seja atribuído a um modelo de pluma convencional. Neste sentido, os autores sugerem a presença de uma pluma com condutos disseminados que utilizam estruturas preexistentes para intrusão das rochas alcalinas, o que é reforçado pela orientação destes corpos magmáticas (maciços e diques).

Palavras-chave: Província alcalina; Datação $^{40}Ar/^{39}Ar$; Datação U-Pb

1 Introduction

The Brazilian Platform has over 100 alkaline intrusion occurrences in its central-southeastern part, presenting mesozoic and cenozoic ages. Gomes & Comin-Chiaramonti (2005) linked these rocks to mobile belts from the Brasiliano Cycle intruded at the Paraná Basin margins, whose emplacement is controlled by regional extensional tectonics (Figure 1). First grouped by Almeida (1983) into 12 different provinces, the alkaline magmatism of the Brazilian Platform was redefined by Riccomini et al. (2005) based on geological, structural, and geophysical data into 15 provinces: Alto Paraguay, Ponta Grossa Arch, Valle Chico, Misiones, Central Paraguay, Amambay, Rio Apa, Rondonópolis Anteclise, Minas-Goiás, Serra do Mar, Piratini, Asunción, Cabo Frio Magmatic Lineament, Velasco and Candelária. Riccomini et al. (2005) suggest subdividing the Serra do Mar Province (SMP) into northern, central, and southern sectors, corresponding to the most significant areas of Cenozoic uplift along the southeastern Brazilian coast. Additionally, these authors also identified the Cabo Frio Magmatic Lineament, also known as the Poços de Caldas – Cabo Frio Alkaline Alignment (PCCFA), as a distinct province. However, other researchers, such as Guarino et al. (2019), continue to regard the PCCFA as part of the northern sector of the SMP.

The SMP – PCCFA contain alkaline complexes and dike swarms, which intrude into the Proterozoic metamorphic terrains of the Ribeira Belt. These intrusions are structurally related to a fault system of the Brasiliano cycle, with ENE to EW trend (Almeida, 1983; Brotzu et al., 2005; Hackspacher & Godoy, 1999; Heilbron et al., 2016). This alkaline magmatism occurred from the Late Cretaceous to the Paleocene, along the ENE-EW transcurrent systems reactivated during the Gondwana break-up (Enrich et al., 2005; Guarino et al., 2019). According to Santos & Hackspacher (2021 and references therein), oceanic fracture zones (FZ; Figure 2A) represent areas of lithospheric weakness perpendicular to the Mid-Ocean Ridge, with faults that exhibit strike-slip movement and contain multiple intrusions linked to mantle plumes. These FZ extend into the continental crust and may be associated with the genenis of dike swarms (e.g., Florianópolis and Pariquera-Açu). In this onshore context, the FZ is also linked with the Southeast Brazilian Meso-Cenozoic tectomagmatism, including the PCCFA.

This paper compiles and presents previously published data on the PCCFA, focusing on petrochronological aspects of alkaline massifs and other magmatic bodies, such as dikes. This review facilitates correlating the alkaline complexes' genesis with existing models (fault reactivation and mantle plumes) to unravel the emplacement of the PCCFA complexes. Additionally, new $^{40}Ar/^{39}Ar$ and U-Pb data for Tinguá and Itatiaia massifs, covering various syenitic facies (amphibole- and biotite-bearing syenite and biotite- and amphibole-bearing nepheline syenite), as well as U-Pb data for monzonite from Morro dos Gatos Hill, are presented to support this investigation.

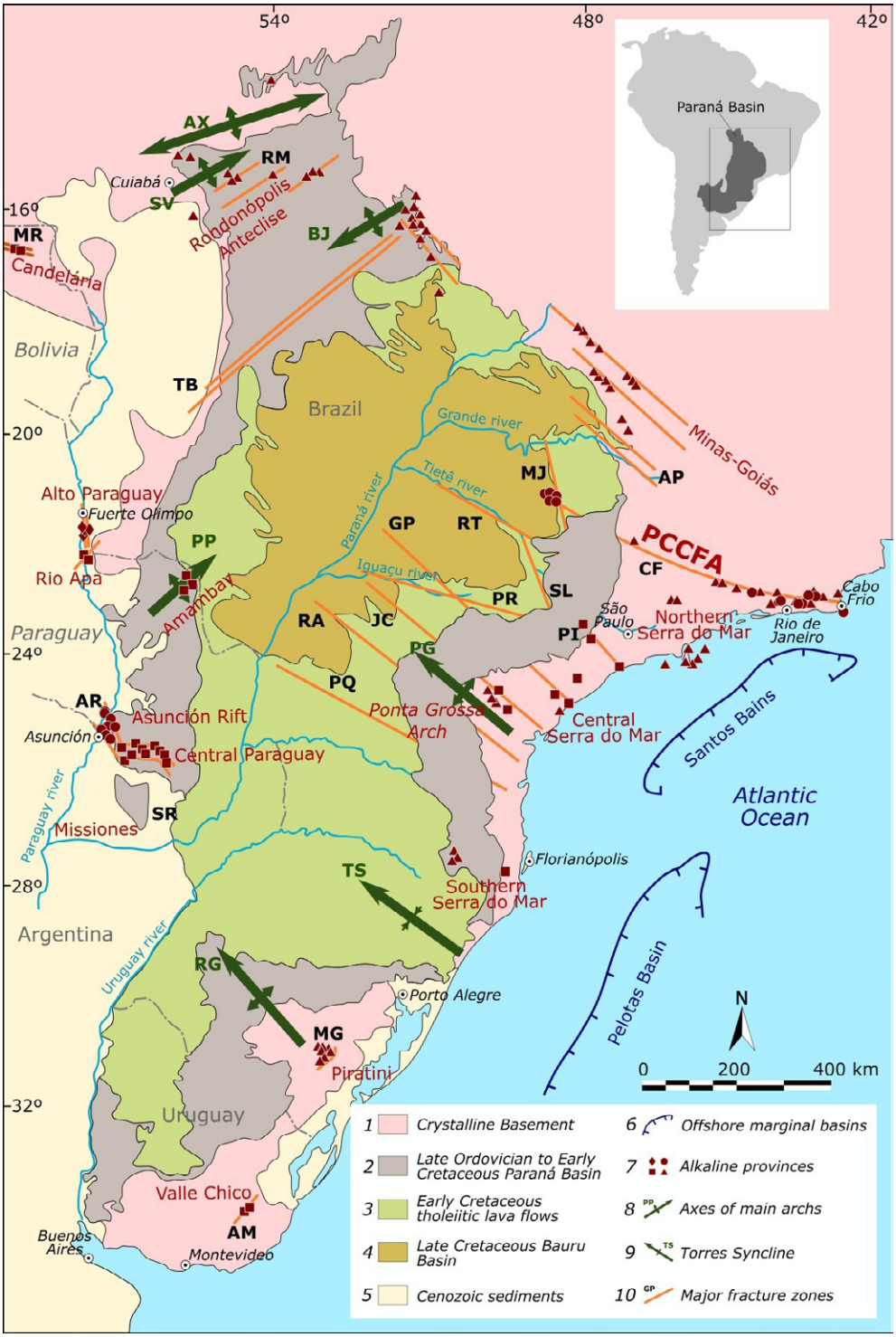

Figure 1 Brazilian Platform map of the central-southeastern region's alkaline provinces, associated lithologies, and main structural features. Ages of alkaline rocks (5): Diamonds - Permian-Triassic; squares - Early Cretaceous; triangles - Late Cretaceous; and circles - Paleogene. Main arches (6): AX - Alto Xingu; SV - São Vicente; BJ - Bom Jardim de Goiás; PG - Ponta Grossa; RG - Rio Grande; PP - Ponta Porã. Major fracture zones (8) - Rifts: MR - Mercedes; RM - Rio das Mortes; MG - Moirão; SR - Santa Rosa; AR - Asunción. Lineaments: TB - Transbrasiliano; AP - Alto Paranaíba; MJ - Moji-Guaçu; CF - Cabo Frio; RT - Rio Tietê; SL - São Carlos-Leme; PR - Paranapanema; PI - Piedade; GP - Guapiara; JC - São Jerônimo-Curiúva; RA - Rio Alonzo; PQ – Rio Piquiri; AM - Santa Lucía-Aiguá-Merin), modified from Milani (1997) and Riccomini et al. (2005).

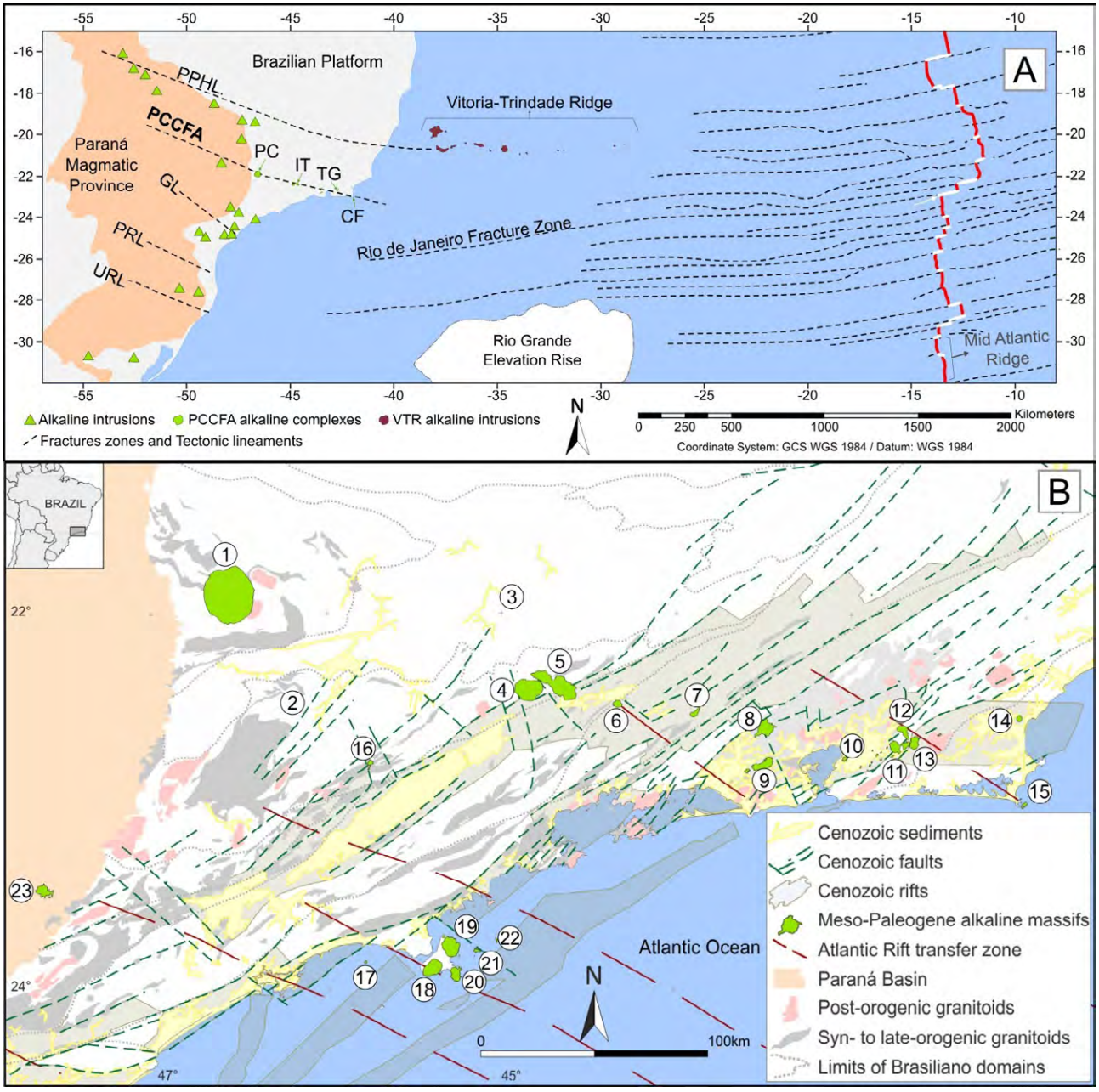

Figure 2 A. Schematic map of southeast Brazil and the southwest Atlantic Ocean, identifying fracture zones, tectonic lineaments, and the Mid-Atlantic Ridge correlating with the alkaline intrusions in the onshore and offshore contexts, modified from Santos & Hackspacher (2021); Lineaments: PPHL - Poxoréu-Paranaíba High lineament; GL – Guapiara lineament; PRL - Piquiri Rive lineament; URL - Uruguay River lineament. Massifs: PC - Poços de Caldas; IT - Itatiaia; TG - Tanguá; CF – Cabo Frio; B. Map of intrusions of the PCCFA and the SMP in the north sector, and regional geological features and structures associated with the southeastern Brazilian Platform. Data were compiled from the CPRM public database, and the map was modified based on Rosa & Ruberti (2018) and Thompson et al. (1998). Alkaline massifs: 1 - Poços de Caldas; 2 - Bom Repouso; 3 - Caxambú; 4 - Passa Quatro; 5 - Itatiaia; 6 - Morro Redondo; 7 - Serra dos Tomazes; 8 - Tinguá; 9 - Mendanha-Mapicuru; 10 - Itaúna; 11 - Tanguá; 12 - Soarinho; 13 - Rio Bonito; 14 - Morro de São João; 15 - Cabo Frio; 16 - Ponte Nova; 17 - Monte de Trigo; 18 - São Sebastião; 19 - Serraria; 20 - Mirante; 21 - Búzios; 22 - Vitória; and 23 - SMP Ipanema near occurrence.

2 The Poços De Caldas – Cabo Frio Alignment's Definition and Geological Content

The SMP is defined by two alignments with distinct structural characteristics (Enrich et al., 2005): 1) an alignment along the Brazilian coast following the Santos fault; and 2) the Cabo Frio Alignment associated with structural rifting systems. The Precambrian-oriented structures possibly controlled the shapes and directions of these intrusions during emplacement, generating elongated bodies from NE to NNE (Riccomini et al., 2005), which has been confirmed by magnetometry data (Ferreira, 2018).

The PCCFA is a slightly curved magmatic province with a WNW-ESE trend that stretches for about 1,150 km, from Jaboticabal (São Paulo State) to the coastline of Cabo Frio (Rio de Janeiro State). The Alignment has 26 alkaline intrusive centers with stocks, massifs, plugs, and many alkaline dikes (Riccomini et al., 2005). The complexes mainly comprise alkali- and nepheline syenites, with quartz-bearing syenites and granite occurrences (Brotzu et al., 2005). The ages of these alkaline intrusions vary between 84 Ma and 39 Ma (Figure 3, Table 1 and Supplementary Material), indicating a decreasing age from west to east (Rosa, 2017), although nonlinear (Santos & Hackspacher, 2021).

Alkaline dikes in the alignment present two groups with distinct geochemical characteristics (Brotzu et al., 2005): 1) strongly silica-undersaturated (basanites, foidites, and a succession from tephrites to phonolites); and 2) weakly silica-undersaturated (alkali basalts to trachytes). According to Macedo et al. (2022 and references therein), the lamprophyres occur as dykes or sills intruding rocks of the Paleoproterozoic metamorphic basement. These dykes tend to follow structures with NE-SW to ENE-WSW directions and may be related to the parental magmas of more evolved alkaline rocks (e.g., syenites). Furthermore, although rare, locally these dykes may be crosscuted by felsic alkaline dykes (e.g., Cabo Frio Island – Motoki et al. 2008).

2.1 PCCFA Genetic Models

Two models for genesis of the PCCFA are intensely debated. The first model associates the magmatism with a mantle plume activity, suggesting that the intrusions' alignment results from the relative plate movement over the plume (Thompson et al., 1998). This hypothesis is supported by geological events and geochronological data, which suggest a decrease towards the east. According to Thompson et al. (1998), the Tristan and Trindade mantle plumes were beneath or close to southeastern Brazil at *ca.* 135 Ma and *ca.* 85 Ma, respectively, reinforcing this model. Additionally, these authors suggested the existence of a sub-lithospheric plume head with a radius of about 600 km, which started to impact the continental lithosphere in the Cretaceous period.

The second model correlates the alkaline emplacement with reactivation of subcrustal faults and then with lithospheric refertilization (Rocha-Júnior et al., 2020), caused by the mantle's partial melting, followed by the melt infiltration through fracture zones (Almeida, 1991). According to Riccomini et al. (2005 and references therein), this reactivation is linked to the South Atlantic opening in three stages: 1) the rift stage, 2) the ocean stage, and 3) contemporary to the continental taphrogenic basin installation in southeastern Brazil. They concluded that crustal discontinuities control the alkaline magmatism, and its development is linked to the main onshore sedimentary basins (Figure 2B), such as the Taubaté and Resende basins (Thomaz Filho et al., 2005).

3 Methodology

3.1 U-Pb Geochronology

The samples analyzed were selected based on their representativeness of the correlated massif and their low degree of alteration. Additionally, other samples had been selected for analysis; however, it was not possible to obtain zircon grains for the study due to insufficient quantities or the absence of the mineral. Prior to geochronological analysis, petrographic studies were conducted on the selected samples, which will be presented together.

The new geochronological data it was obtained from zircon crystals from rocks processed and prepared in the Geological Sample Processing Laboratory (LGPA) of Rio de Janeiro State University (UERJ). Milling was used to reduce the particle size, followed by magnetic separation (Frantz), to concentrate the mineral of interest (zircon) into a dense liquid. The mineral concentrate was later taken to the Multilab Laboratory at UERJ, where the zircon crystals were collected using a stereomicroscope. The crystals were mounted on an epoxy resin to obtain zircon cathodoluminescence images and conduct the U-Pb analyses.

A New Finningan Neptune MC-ICP-MS system was coupled to an excimer laser ablation device in the Multilab Laboratory for U-Pb analyses. This laser device features a camera that allows conducting a detailed analysis from the ablation of the crystal using a laser spot with a diameter between 80 and 100 μm. For the analyses, the frequency was 5 Hz, and the energy variation was 80% to 100%. Helium gas was used for carriage in the laser ablation, while argon gas was used in ICP-MS. Two different standards were used for the analyses: GJ-1 from Jackson et al. (2004) and 91500 from Wiedenbeck et al. (1995).

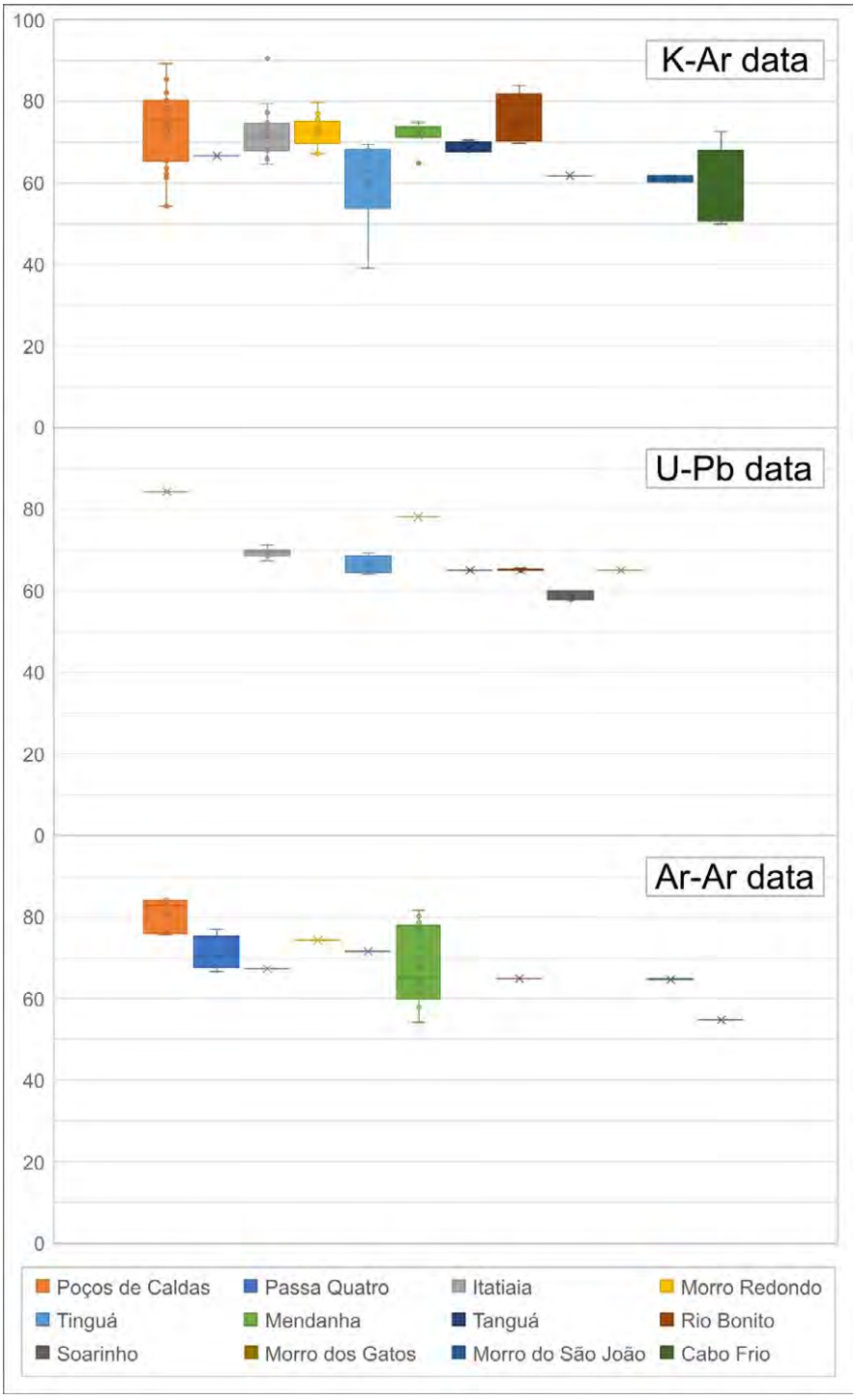

Figure 3 Boxplot diagram of geochronological data of the main PCCFA alkaline complexes arranged from west to east. When the massif has no age obtained by the specific method, its interval is skipped. The $^{40}K/^{40}Ar$ ages are from Amaral et al. (1967), Biondi (2005), Brotzu et al. (1989), Bushee (1971), Montes-Lauar et al. (1995), Ribeiro Filho & Cordani (1966), Sonoki & Garda (1988), Thompson et al. (1998), and Ulbrich et al. (2002). The U-Pb are from Rosa (2017), Silva (2019), Silva et al. (2020, 2023), and Takenaka (2014). The $^{40}Ar/^{39}Ar$ ages are from Brotzu et al. (1992), Deckart et al. (1998), Ferrari (2001), Montes-Lauar et al. (1995), Montes-Lauar & Pacca (1988), Mota (2012), Motoki et al. (2013), Shea (1992), Silva et al. (2015), Silva et al. (2020), Sonoki & Garda (1988), Ulbrich et al. (2002), Vlach et al. (2003), and the present work. See Supplementary Material for details, such as method, used material/rock and the associated reference.

Table 1 Statistical summary of geochronological data for the main PCCFA complexes, considering all analytical methods. Data sources include Amaral et al. (1967), Biondi (2005), Deckart et al. (1998), Ferrari (2001), Mota (2012), Motoki et al. (2013; 2010), Netto et al. (2005), Silva et al. (2018, 2020), Silva (2019), Smith et al. (1999), Sonoki and Garda (1988), Thompson et al. (1998), and from present work (see Supplementary Material for details, such as method, used material/rock and the associated reference). n: number of data; The table provides the following information: the minimum represents the lowest geochronological value for each massif; the median is the central value of the data set when arranged in ascending order; and the maximum represents the highest geochronological value.

Massifs	n	Minimum (Ma)	Median (Ma)	Maximum (Ma)
Poços de Caldas	67	54.2	76.3	89.3
Passa Quatro	4	66.7	70.4	77.0
Itatiaia	26	64.6	69.6	90.5
Morro Redondo	15	67.2	72.6	79.8
Tinguá	8	39.1	66.5	71.6
Mendanha	24	54.2	71.5	81.8
Tanguá	8	65.0	68.2	74.0
Rio Bonito	10	65.0	65.3	83.9
Soarinho	4	58.0	59.0	61.8
Morro dos Gatos	1	65.4	65.4	65.4
Morro do São João	4	60.1	63.1	64.9
Cabo Frio	5	50.0	54.0	72.4

3.2 $^{40}Ar/^{39}Ar$ Radioisotopic Data

Fresh biotite from the nepheline syenite of the Itatiaia Complex and amphibole from the syenite of the Tinguá Complex were selected. These minerals were separated using a Frantz magnetic separator and then hand-picked under a stereomicroscope. The selected amphibole minerals were leached in diluted HF for one minute and then thoroughly rinsed with distilled water in an ultrasonic cleaner.

Samples were loaded into two large aluminum disc wells. These wells were bracketed by small wells, including Fish Canyon sanidine used as a neutron flux monitor, for which an age of 28.03 ± 0.08 Ma was adopted (Jourdan & Renne, 2007). The discs were Cd-shielded (to minimize undesirable nuclear interference reactions) and irradiated for 25 hours in Hamilton University's McMaster nuclear reactor (Canada) in position 5C. The J-values were 0.0091820 ± 0.0000266 (Tinguá Complex) and 0.0090200 ± 0.0000496 (Itatiaia Complex). Mass discrimination was monitored using an automated air pipette, which indicated a mean value of 1.00583 ± 0.00322 per dalton (atomic mass unit). The correction factors for interfering isotopes were $(^{39}Ar/^{37}Ar)_{Ca} = 7.30x10^{-4}$ (± 11%), $(^{36}Ar/^{37}Ar)_{Ca} = 2.82x10^{-4}$ (± 1%) and $(^{40}Ar/^{39}Ar)_{K} = 6.76x10^{-4}$ (± 32%).

The $^{40}Ar/^{39}Ar$ analyses were performed at the Western Australian Argon Isotope Facility of Curtin University. The amphibole aliquot was step-heated using a 110 W Spectron Laser System, with a continuous Nd-YAG (IR; 1064 nm) laser rastered across either single large grains or multigrain aliquots wrapped in zero-blank niobium foil, throughout approximately 1 mn to ensure a homogeneously distributed temperature. The biotite aliquot was step-heated in a double vacuum high-frequency Pond Engineering furnace. The gas was purified in a stainless steel extraction line using three SAES AP10 getters and a liquid nitrogen condensation trap. Ar isotopes were measured in static mode using an MAP 215-50 mass spectrometer (resolution of *ca*. 450; sensitivity of $4x10^{-14}$ mol/V) with a Balzers SEV 217 electron multiplier, mostly using 9 to 10 peak-hopping cycles. The data acquisition was performed using the Argus program by M.O. McWilliams and was run under a LabView environment.

The raw data were processed using the ArArCALC software (Koppers, 2002), and the ages were calculated using the decay constants recommended by Renne et al. (2011). Blanks were monitored every 3 to 4 steps. All parameters and relative abundance values are provided in the Supplementary Material.

4 Results

4.1 PCCFA Complex Review and New Geochronological Data

Based on recent works, we compiled geological, petrographic, mineralogical, and geochronological data for the PCCFA alkaline complexes. The data are presented according to their geographical position, from west to east, in the following sections. The main rock types found in each massif and their associated mineralogy are summarized in Table 2, while the lithogeochemical, geochronological, and isotopic data are provided in the Supplementary Material.

4.1.1. Poços de Caldas Complex (MG)

The Poços de Caldas Complex (Figure 4A) is circular and the largest in Brazil (*ca.* 800 km² – Ulbrich et al., 2005). The massif comprises nepheline syenites and phonolites, with relevant quantities of strongly agpaitic rock types, pyroclastic rocks, and remnants of lava flows, the last being formed by mafic-ultramafic rocks from the Serra Geral Formation (Ulbrich et al., 2005). Nepheline syenite rocks are medium- to coarse-grained, generally with hypidiomorphic textures, and contain large and microperthitic alkali feldspar macrocrystals (oikocrysts), which enclose different chadacrysts such as nepheline, clinopyroxene and titanite among others. Nepheline syenites' major minerals consist of alkali feldspar, nepheline and clinopyroxene (aegirine to sodic augite), and the main accessory phases are sodalite, amphibole, titanite, apatite, biotite and eudialyte. The phonolites are texturally diverse, presenting subaphyric to seriate porphyritic characteristics, with fine-grained to medium-grained groundmass. Alkali feldspar and nepheline are the main phenocrysts, but clinopyroxene and amphibole are also observed (Guarino et al., 2021).

The first geochronological study yielded ages between 87 and 109 Ma and was performed on zircon crystals from phonolitic dikes that cross-cut nepheline syenites using the lead-alpha method (Dutra, 1966). The several rocks analyzed by Ulbrich et al. (2002) showed $^{40}K/^{40}Ar$ ages ranging from 54.2 to 89.3 Ma. The Rb/Sr data (whole-rock) showed isochron ages of 78.6 ± 6.6 Ma for nepheline syenites and 76.6 ± 2.6 Ma for hydrothermally altered syenite (Ulbrich et al., 2002). Shea (1992) presented two $^{40}Ar/^{39}Ar$ readings of biotite from a lamprophyre dike, which crosscut phonolites and syenites, which are the primary rocks of the massif, and even breccias in the Osamo Utsumi Mine. These analyses yielding ages of 75.6 ± 0.6 and 76.2 ± 1.6 Ma from mica phenocryst and groundmass mica, respectively. The $^{40}Ar/^{39}Ar$ plateau ages were determined for a phlopogite from carbonatitic dikes, which is a late hydrothermal veins, varying between 83.5 ± 0.1 Ma and 84.3 ± 0.1 Ma. These data suggesting a minimum age for mineral crystalization and vein formation (Vlach et al., 2003). See Supplementary Material for details of these geochronological data.

4.1.2. Passa Quatro Complex

The Passa Quatro Complex (*ca*. 165 km²) has a subcircular geometry and consists of a ring- and plug-like body (Chiessi, 2004; Guarino et al., 2019), featuring more silica-undersaturated and peralkaline rocks than the Itatiaia Complex itself (Guarino et al., 2019). The complex predominantly comprises nepheline syenites, which are intruded by alkaline polymictic breccias and phonolite dikes. The nepheline syenite is medium to coarse-grained and has hypidiomorphic to slightly porphyritic textures. The mineral composition includes alkali feldspar and variable amounts of nepheline, with plagioclase occurring in some rocks. Mafic minerals such as amphibole, pyroxene, and biotite occur as accessories, and sodalite and analcime are rare (Brotzu et al., 1992; Enrich et al., 2005; Guarino et al., 2019). Locally cumulus or flow textures involving large alkali feldspar grains

According to Enrich et al. (2005), the phonolite dikes can be divided into three types based on texture and mineralogy. The first type has an aphanitic texture and contains sanidine, nepheline, clinopyroxene, amphibole, and titanite as the main minerals. The second type exhibits a porphyritic texture with phenocrysts of sanidine, biotite, opaque minerals, and occasional pseudoleucite, along with apatite and titanite as accessory minerals (miaskitic type). Lastly, the third type is also porphyritic, featuring phenocrysts of sanidine and nepheline, with clinopyroxene, amphibole, and titanite in a matrix of similar mineralogy (agpaitic type).

Few geochronological analyses have been reported regarding the Passa Quatro Complex. The $^{40}K/^{40}Ar$ age in amphibole from nepheline syenite yielded an age of 66.7 ± 3.3 Ma (Ribeiro Filho & Cordani, 1966, recalculated by Sonoki & Garda, 1988). The Rb-Sr isochron (whole-rock) showed an age of 70.43 ± 0.5 Ma (Montes-Lauar et al., 1995) and an age of 77 ± 3 Ma (Brotzu et al., 1992), both performed in nepheline syenites. The details of these data are in the Supplementary Material.

Table 2 Summary of the main lithologies observed in the primary massifs of the PCCFA, along with their major and accessory minerals. This information was compiled from studies by Brotzu et al. (1989, 1992, 2007); Enrich et al. (2005); Geraldes et al. (2013); Guarino et al. (2019; 2021); Mota (2012); Motoki et al. (2010, 2013); Rosa & Ruberti (2018); Silva et al. (2015); Silva et al. (2018, 2023); Silva (2019); Silveira et al. (2005); and Valença (1980).

Massif	Main rocks	Minerals	
		Major	Accessory
Poços de Caldas	Nepheline syenite, phonolite and pyroclastic rocks	Alkali feldspar, nepheline and clinopyroxene	Sodalite, amphibole, titanite, apatite, biotite, and eudialyte
Passa Quatro	Nepheline syenite, breccia and phonolite	Alkali feldspar, nepheline, plagioclase, amphibole, pyroxene, biotite	Titanite, apatite, Ti-magnetite, låvenite, and eudialyte
Itatiaia	Syenite, nepheline syenite, phonolite, nephelinite, nordmarkite, granite, trachyte, monzonite, trachybasalt, and melagabbro	Alkali feldspar, nepheline, clinopyroxene, amphibole, biotite, titanite, apatite, zircon, titanomagnetite, sodalite, quartz (in quartz syenites)	Ilmenite, låvenite, hiortdahlite, astrophyllite, and catapleiite
Morro Redondo	Alkali syenite, nepheline syenite, trachyte, and phonolite	Alkali feldspar and nepheline	Nepheline, plagioclase, hornblende, biotite, titanite, apatite, and opaques
Tinguá	Syenite, nepheline syenite and phonolite	Alkali feldspar and nepheline	Amphibole, titanite, apatite, and opaques
Mendanha	Syenite, trachyte, breccia, lapillite, and phonolite	Alkali feldspar, nepheline, plagioclase, and hornblende	Biotite, scapolite, muscovite, carbonate, zircon, apatite, augite, and opaque
Tanguá	Syenite, nepheline syenite, breccia, trachyte and phonolite	Alkali feldspar, nepheline, amphibole, and biotite	Magnetite, titanite and apatite
Rio Bonito	Syenite, nepheline syenite, breccia, trachyte and phonolite	Alkali feldspar and nepheline	Hornblende, clinopyroxene, biotite, opaques, titanite, apatite, and zircon
Soarinho	Syenite, quartz syenite, quartz monzonite, breccia and nordmarkite	Alkali feldspar, plagioclase and biotite	Quartz (in quartz-bearing rocks), amphibole and opaque
Morro dos Gatos	Alkaline syenite, nepheline syenite, monzonite, trachyte, gabbros and pyroclastic rock	Alkali feldspar, plagioclase, clinopyroxene, and biotite	Quartz, apatite and magnetite
Morro do São João	Alkaline syenite, nepheline syenite, clinopyroxenite and alkaline gabbro	Alkali feldspar and nepheline	Biotite, amphibole, clinopyroxene, titanite, apatite, Ti-magnetite and melanite garnet
Cabo Frio	Alkaline syenite, nepheline syenite, phonolite, trachyte, and breccia	Alkaline feldspar, nepheline, clinopyroxene, amphibole, and biotite	Magnetite, titanite and apatite

4.1.3. Itatiaia Complex

The Itatiaia complex (*ca.* 215 km^2) has a roughly NW-SE ellipsoidal body (Figure 4B) with an association of plug- or dike-type intrusions in the complex's external part (Melluso et al., 2017), as well as moon-shaped units (Rosa & Ruberti, 2018). According to these last authors, the intrusion can be subdivided into three sectors based on the association of structures and lithotypes: Southeastern Sector (SE-S), Central Sector (C-S), and Northwest Sector (NW-S).

The SE-S comprises nepheline syenites, biotite hornblende nepheline syenite, sodalite nepheline syenite, and aegirine nepheline foyaitic syenite, with miaskitic to agpaitic signatures, besides dikes of phonolite and nephelinite. The C-S has a ring-like structure, which was intruded in part of the southeastern sector, with a neck-like structure formed in the transition area to the northwestern sector. The sector shows nepheline syenite (with an agpaitic assemblage), nordmarkite, alkali feldspar granite, quartz alkali feldspar syenite, and trachytes. The NW-S comprises quartz and nepheline syenites, trachytes, monzonite, trachybasalt, and a metasomatized cumulative melagabbro with an unclear structure and intrusion relationships (Rosa & Ruberti, 2018).

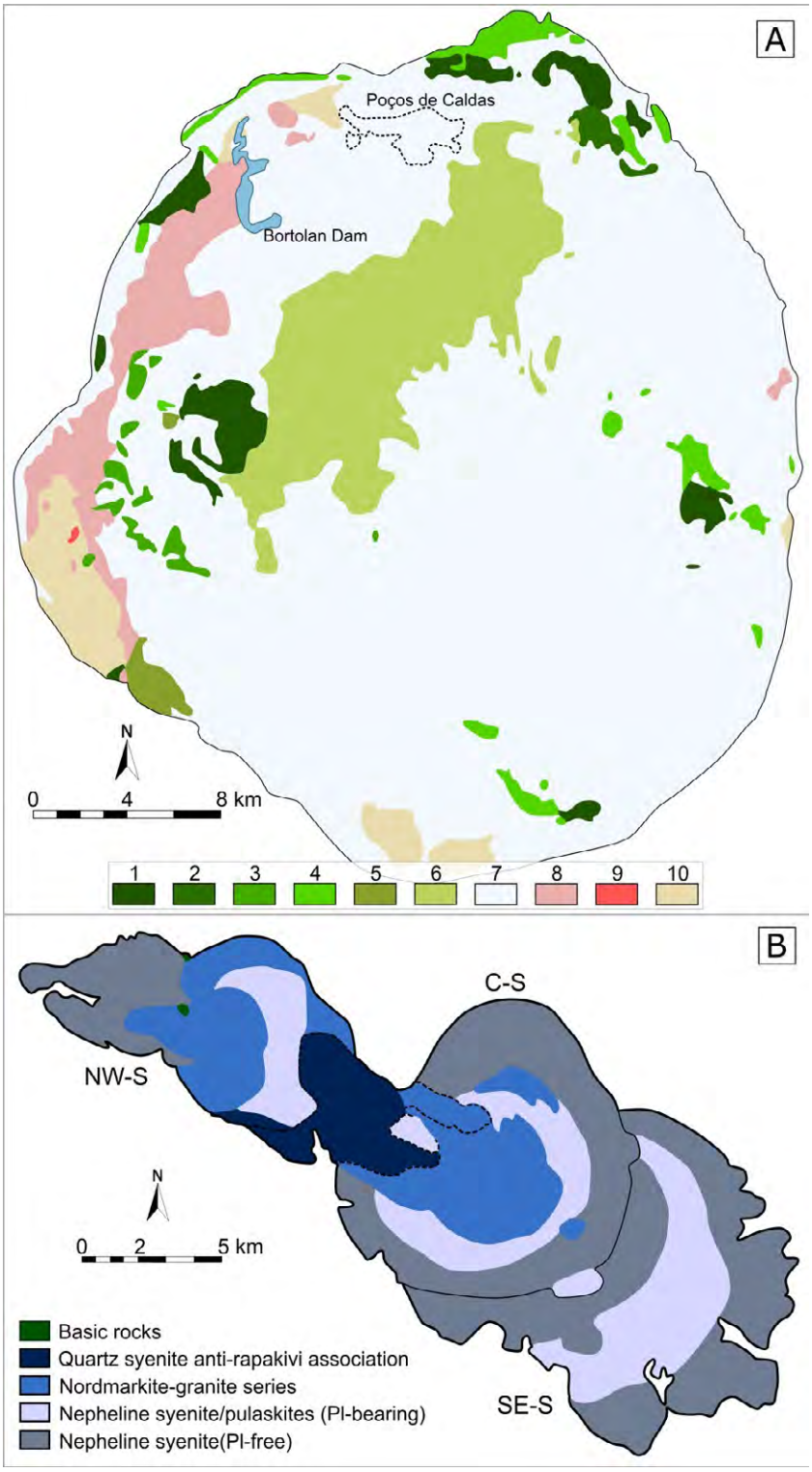

Figure 4 A. Simplified Poços de Caldas Complex geological map, modified from Ulbrich et al. (2005). The lithologies are 1) agpaític nepheline syenite; 2) nepheline syenite with pseudoleucite; 3) porphyritic nepheline syenite; 4) gray nepheline syenite; 5) biotite-bearing nepheline syenite; 6) nepheline syenite; 7) tinguaites and phonolites, undifferentiated; 8) volcaniclastic deposits; 9) diabase; 10) sandstones and related sedimentary rocks; B. Simplified map of the Itatiaia alkaline massif with sectors, modified from Rosa & Ruberti (2018).

According to Rosa & Ruberti (2018), the nepheline-bearing syenites comprise nepheline, alkali feldspar, clinopyroxenes, hornblende, biotite, titanite, apatite, zircon, titanomagnetite, sodalite and ± ilmenite. The agpaitic minerals locally observed are låvenite, hiortdahlite, astrophyllite, and catapleiite, with arfvedsonite and aegirine. Quartz-bearing syenites comprise mainly quartz, alkali feldspar, clinopyroxene, richterite/ferro-richterite, biotite, titanite, and titanomagnetite. Apatite, ilmenite and chevkinite can be observed.

The first geochronological analyses were carried out by Amaral et al. (1967 and recalculated by Sonoki & Garda, 1988), and have an average age of 68 Ma ($^{40}K/^{40}Ar$ age), using biotite (5) and barkevikite (1) from nepheline- and quartz syenites. Other $^{40}K/^{40}Ar$ data varied between 64.6 ± 1.0 and 90.5 ± 2.2 Ma and were obtained using different minerals of nepheline syenites (Sonoki & Garda, 1988). More recent studies obtained from U-Pb data (zircon) yielded ages varying between 71.26 ± 0.29 to 67.47 ± 0.25 Ma, using several syenites (Rosa, 2017). See Supplementary Material for details.

4.1.4. Morro Redondo Complex

The Morro Redondo Complex (*ca.* 8 Km²) has a subcircular shape. Valença et al. (1983) indicated a mineral zoning for syenitic mass. The central zone has slightly high proportions of nepheline and amphiboles compared to the outermost zones (Brotzu et al., 1989).

The complex comprises syenites (nepheline- and alkali- with nepheline) and trachytic to phonolitic breccias (Mota, 2012). Nepheline syenites are medium- to coarse-grained rocks and locally show inequigranular or cumulatic textures (Brotzu et al., 1989; Mota, 2012). The main mineral is K-feldspar in ripiform euhedral crystals, while plagioclase and hornblende are also observed. Nepheline-bearing alkali syenites are coarse-grained and have cumulatic (Brotzu et al., 1989) and inequigranular textures. K-feldspar is the main mineral present in these rocks (*ca*. 75%), but hornblende, biotite, nepheline, titanite, apatite, and opaques are also observed. Trachytes have a porphyritic texture with aphanitic groundmass and K-feldspar phenocrysts. The groundmass comprises K-feldspar, clay minerals, opaques, and apatite. Xenoliths and iron oxides surrounding vugs can also be found in the trachytes (Mota, 2012).

The $^{40}K/^{40}Ar$ age in amphibole from nepheline syenites yielded an age of 67.2 ± 4.0 Ma for the Morro Redondo Complex (Ribeiro Filho & Cordani, 1966, recalculated by Sonoki & Garda, 1988). Brotzu et al. (1989) analyzed biotite, amphibole, and whole-rock from syenites, alkali- and nepheline syenites, and phonolites. The study yielding $^{40}K/^{40}Ar$ ages between 68.0 ± 4.9 Ma and 79.8 ± 3.4 Ma. Additionally, hornblende $^{40}Ar/^{39}Ar$ data obtained from nepheline syenites yielded an age of 74.38 ± 0.50 (2σ) Ma (plateau age – Mota, 2012). See Supplementary Material for details.

4.1.5. Tinguá Complex

The Tinguá Complex (*ca. 50* km²) with subcircular shape and the massif comprises syenites and phonolites. Nepheline syenite is a coarse-grained rock composed of K-feldspar and nepheline, with amphibole, titanite, apatite, and opaques as accessories. Phonolite is fine-grained, even microcrystalline-grained, and has a microporphyritic texture. Ripiform K-feldspar phenocrysts and square/hexagonal nepheline are observed, and acicular amphibole, opaques, and titanite occur as accessories (Silva, 2019). Some earlier studies (e.g. Sonoki and Garda, 1988) refer to the presence of a rock type called tinguaite (as in other massifs of the PCCFA), although this term is now obsolete. The term was introduced by Rosenbusch in 1887 to describe the texture of a subvolcanic phonolite composed of alkali feldspar, nepheline with or without other feldspathoids, aegirine, and sometimes biotite (Le Maitre et al., 2002; Ulbrich et al., 2005).

The $^{40}K/^{40}Ar$ analyses yielded ages of 60.1 ± 2.6 Ma (mafic minerals) and 67.9 ± 3.9 Ma (biotite), both performed on nepheline syenite (Amaral et al., 1967, recalculated by Sonoki & Garda, 1988). These last authors also showed a $^{40}K/^{40}Ar$ date of 39.1 ± 3.4 Ma based on whole-rock analysis of tinguaite (phonolite). The U-Pb ages in zircons from nepheline syenites yielding ages of 67 ± 4 Ma, 64 ± 2 Ma, and 66 ± 3 Ma (Silva, 2019). All these ages are in the Supplementary Material.

4.1.6. Mendanha Complex

The Mendanha Complex (Figure 5A) is formed by morphological elevations, and two main intrusions are observed: 1) the Mendanha alkaline massif and 2) the Marapicu massif. The Mendanha massif comprises syenites embedded in gneisses and different types of porphyritic trachytes, breccias, lapillites, and agglomerates. Trachytic lavas intercalated with breccias in subhorizontal layers and pumps with sudden cooling surfaces are observed, suggesting mixed magmatism (Silveira et al., 2005).

The Marapicu lithotypes are classified into two facie categories: 1) syenitic and 2) phonolitic. The syenitic facies comprise alkali feldspar, nepheline, plagioclase,

and hornblende. Biotite, scapolite, muscovite, carbonate, zircon, apatite, augite, and opaque (mainly magnetite) are accessory minerals. The phonolitic facies are divided into two groups based on phenocryst contents: the first one is represented by phenocrysts of alkali feldspar, nepheline, and hornblende; the second one is composed of phenocrysts of sanidine and nepheline, with some occurrences of biotite phenocrysts (Silva et al., 2015).

The $^{40}K/^{40}Ar$ dating of hornblende, biotite and groundmass range from 64.9 ± 1.6 to 74.9 ± 3.3 Ma (Sonoki & Garda, 1988). Fission track data showed an age range of 65.3 Ma to 66.5 Ma (Netto et al., 2005). According to Mota (2012), the $^{40}Ar/^{39}Ar$ analyses yielded an age of 64.12 ± 0.40 (2σ) Ma of biotite (plateau age) and an age of 58.55 ± 0.45 Ma for a lamprophyre dike (whole-rock - plateau age). Other $^{40}Ar/^{39}Ar$ age studies were carried out in different minerals (hornblende, biotite, and phlogopite, or whole-rock), yielding ages varying between 54.2 ± 2.8 and 81.8 ± 1.8 Ma (Deckart et al., 1998; Ferrari, 2001; Smith et al., 2001). Detailed geochronological data can be found in the Supplementary Material.

4.1.7. Tanguá Complex

The Tanguá Complex (*ca.* 50 Km²) comprises syenites, volcanic breccias and dikes of trachyte and phonolite (Motoki et al., 2010). Valença (1980) proposed a concentric division according to its mineralogical and textural characteristics, split into lower, middle, and upper syenite, besides the brecciated zones. The lowest zone is in contact with the metamorphic basement, has no pseudoleucite, and has the lowest content of nepheline, while both increase toward the upper zone. Similar behaviors are observed for textural features towards the center. On the other hand, the content of orthoclase, biotite, and plagioclase decreases towards the upper zone.

Nepheline syenites are coarse-grained, with alkali feldspar, nepheline and amphibole as the main minerals, while magnetite, titanite and apatite occur as accessories (Motoki et al., 2010). Alkaline syenites have a porphyritic texture with alkali feldspar phenocrysts, and also comprise nepheline, amphibole, and biotite, with magnetite, titanite, and apatite as accessories (Motoki et al., 2010). Phonolite is observed as dikes, crosscutting syenitic bodies, or tabular xenoliths in the nepheline syenite magma (Motoki et al., 2010). Fluorite-bearing hydrothermal veins, often parallel to the dikes, are observed in the massif (Silva et al., 2018).

The $^{40}K/^{40}Ar$ ages are 68.4 ± 2.3 Ma (amphibole) and 67.8 ± 1.9 Ma (K-feldspar), both from syenite (Cordani & Teixeira, 1979, recalculated by Sonoki & Garda, 1988). The Rb-Sr whole-rock analyses yielded an intrusive age of 66.8 Ma for a nepheline syenite (Motoki et al., 2010). Silva et al. (2018) used the (U-Th)/He method with fluorites from hydrothermal veins to obtain hydrothermal ages between 0.11 ± 0.02 Ma and 74.1 ± 2.8 Ma. The U-Pb analyses of zircon crystals from nepheline syenite yielded an age of 65 ± 1 Ma (2σ – Silva, 2023). The Supplementary Material provides more details regarding the geochronological data.

4.1.8. Rio Bonito Complex

The Rio Bonito Complex (*ca.* 29 km²) exhibits concentric zoning with lower, middle, and upper syenitic facies (Valença, 1980). In the lower zones outcrops syenites with lower nepheline content and higher orthoclase content. The upper zone, however, consists of syenite richer in nepheline, making this massif zoning similar to Tanguá Complex. Additionally, magmatic breccias are exposed in the western portion of the massif.

The massif comprises nepheline syenite and alkali feldspar syenite, dikes of trachyte and phonolite crosscutting the others lithotypes, and volcanic breccias (Silva et al., 2020). Nepheline syenites, the main rock types in the complex, are coarse-grained and comprise alkali feldspar and nepheline as major minerals and hornblende, clinopyroxene, biotite, opaques, titanite, apatite, and zircon as accessories. The alkali syenite without nepheline is mainly found in the intrusion borders and the subvolcanic breccias outcrop in the western part of the massif (Valença, 1980).

The first results of $^{40}K/^{40}Ar$ analyses of K-feldspars varied between 69.7 Ma and 83.9 Ma from nepheline syenite (Amaral et al., 1967, recalculated by Sonoki & Garda, 1988). The U-Pb analyses of zircon crystals from nepheline syenite yielded ages of 65.47 ± 0.60 Ma and 65.18 ± 0.60 Ma (Silva et al., 2020). The $^{40}Ar/^{39}Ar$ dating showed similar results, yielding ages of 65.03 ± 0.70 Ma (biotite) and 65.03 ± 0.46 Ma (amphibole), both from nepheline syenite (Silva et al., 2020). For additional information on the geochronological data, see the Supplementary Material.

4.1.9. Soarinho Complex

The Soarinho Complex is mildly silica-oversaturated to saturated and is split into two zones: 1) the north zone (W-E orientation), which is composed of quartz-bearing syenites, quartz-bearing monzonite, and less saturated syenites; and 2) the south zone (N-S orientation), which comprises breccias and saturated syenites (Valença, 1980). According to Sonoki & Garda (1988), some rocks are described as nordmarkite.

The quartz syenites have porphyritic textures and fine- to medium-grained matrix with coarse phenocrysts (rounded orthoclase phenocrysts and plagioclase laths). Monzonites are medium- to coarse-grained rocks with mesocratic characteristics and comprise plagioclase, K-feldspar, and biotite as major minerals and quartz as accessory. The alkali-feldspar syenite is medium- to coarse-grained, mainly composed of anhedral to ripiform K-feldspar, with amphibole and opaque minerals as accessories (Silva et al., 2023).

The $^{40}K/^{40}Ar$ aging (biotite) of nordmarkite yielded a result of 61.8 ± 2.5 Ma (Cordani & Teixeira, 1979, recalculated by Sonoki & Garda, 1988). The U-Pb ages using zircon crystals are 58 ± 2 Ma for quartz syenite, 60 ± 2 Ma for monzonite, and 58 ± 2 Ma for alkali-feldspar syenite (Silva et al., 2023). See Supplementary Material for details.

4.1.10. Morro dos Gatos Alkaline Hill

The Morro dos Gatos Alkaline Hill (less than 0.5 km² – Monteiro, 2021) is a semicircular outcrop (Figure 5B), with rocks showing a varying concentric shape (alkaline gabbros) towards the core (biotite syenites – Monteiro, 2021). According to Geraldes et al. (2013), the Morro dos Gatos body intrudes into the Silva Jardim granite, most of the hill, while the alkaline rocks outcrop in the western portion.

This latter portion consists of rocks that range from syenite to monzonite, characterized by coarse grain size, equigranular texture, and the absence of evident mineral orientation. Trachyte occurs in two generations: the first is found in the western portion and its abrupt contact with other rocks indicates that this rock is not associated with a lava flow or dike; the second is associated with dikes that cut through the main intrusion. Breccia dikes are also observed cutting through the Morro dos Gatos body (Geraldes et al., 2013).

The same authors indicate that the alkaline rocks of the massif are primarily composed of alkali feldspar, plagioclase, clinopyroxene, and biotite, with quartz, apatite, and magnetite occurring as accessory minerals. Additionally, nepheline and amphibole are not found. No previous geochronological studies have been conducted on the alkaline rocks of the Morro dos Gatos Complex.

4.1.11. Morro do São João Alkaline Complex

The Morro de São João Alkaline Complex (MSJ – *ca.* 10 km²) has circular shape (Figure 5C) and conical body with *ca*. 4 km diameter, with the top dissected by weathering processes. Fagundes (2020) proposed a magmatic faciological map of the MSJ, which presents three main facie types 1) leucocratic facies, 2) mesocratic facies (with mingling features), and 3) melanocratic facies.

The complex mainly comprises melanocratic nepheline syenites (shonkinite) and nepheline syenites, subordinate clinopyroxenites, and alkaline gabbros (Brotzu et al., 2007). The melanocratic nepheline syenites and nepheline syenites are crosscut by thin tabular intrusions, ranging from phonotephrite to phonolitic compositions, while the mafic-ultramafic rocks are classified as cumulates. The cumulate rocks have clinopyroxene, apatite, titanite, and Ti-magnetite as cumulus phases, and the intercumulus phases are biotite, amphibole, alkali feldspar, and nepheline (< 1 vol%). The alkali gabbros have less clinopyroxene, apatite, titanite, and Ti-magnetite. The felsic phases include plagioclase as an early phase and alkali feldspar as interstitial minerals. The felsic rocks are alkali syenites and nepheline syenites and comprise interstitial nepheline and alkali feldspar with rare plagioclase cores. The accessory phases are titanite, apatite, Ti-magnetite, and melanite garnet.

The $^{40}K/^{40}Ar$ data indicated an age of 61.6 ± 1.5 Ma for nepheline syenite whole-rock and an age of 60.1 ± 2.1 Ma using K-feldspar from malignite (Amaral et al., 1967, recalculated by Sonoki & Garda, 1988). Mota (2012) reported a $^{40}Ar/^{39}Ar$ age of hornblende from nepheline syenite of 64.86 ± 0.61 Ma. See Supplementary Material for details.

4.1.12. Cabo Frio Island

The Cabo Frio Island (Figure 5D) is the easternmost complex and comprises nepheline syenite and alkaline syenite plutons, which are crosscut by phonolite, trachyte, lamprophyre dikes, and subvolcanic breccia (Motoki et al., 2013). According to these authors, the main rock in the massif is coarse-grained nepheline syenite, which comprises alkaline feldspar, nepheline, clinopyroxene, amphibole, and biotite as major minerals, with magnetite, titanite and apatite accessories. The alkaline syenite has similar major minerals, including alkali-feldspar, clinopyroxene and amphibole. Additionally, it is worth noting that host rock xenoliths show signs of plastic deformation.

Another rock linked to Cabo Frio Island is the pulaskite (nepheline-bearing alkali feldspar syenite – Le Maitre et al., 2002). This lithotype is described as a medium-grained rock, with alkali feldspar and biotite as the main minerals, and smaller amounts of barkevikite, sodalite, and nepheline. Apatite, sphene, and magnetite occur as accessory minerals (Amaral et al., 1967). The pyroclastic body of Cabo Frio Island is a subvolcanic conduit (Sichel et al., 2008), which is heavily weathered (Motoki et al., 2008).

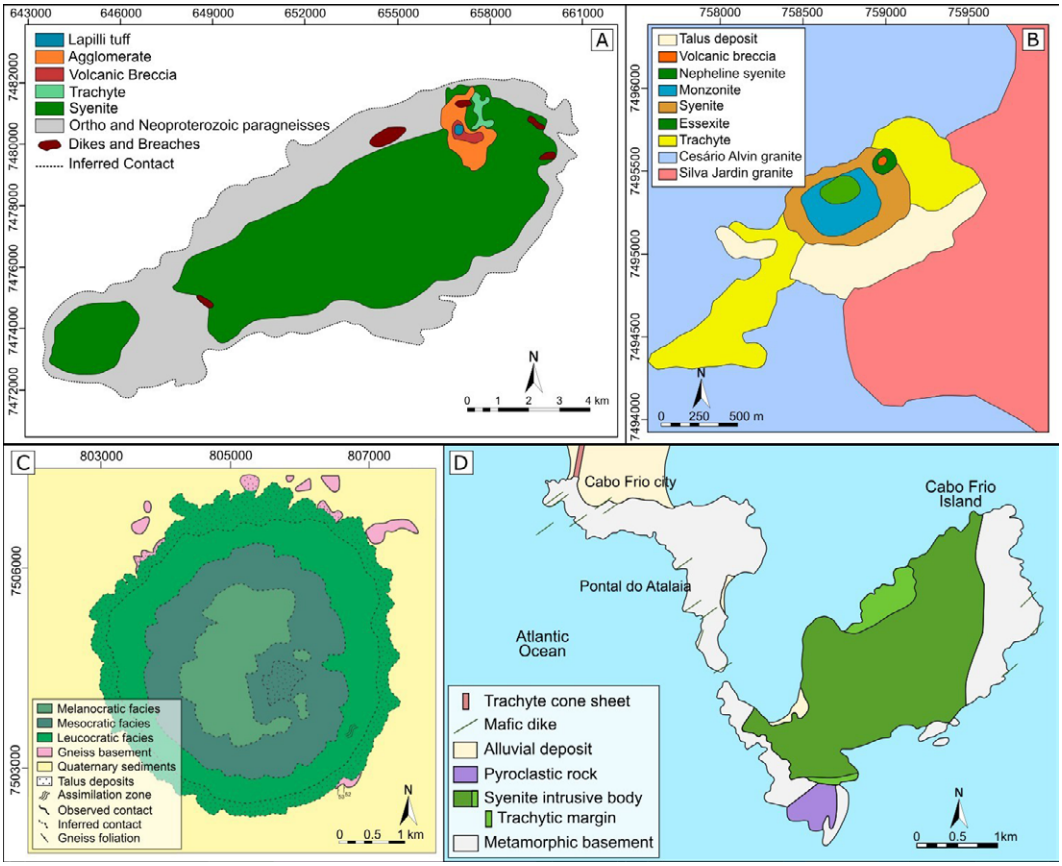

Figure 5 A. Geological map of the Mendanha Complex, modified from Mota (2012); B. Morro dos Gatos Alkaline Hill Geological map, modified from Monteiro (2021); C. Magmatic facie map of the Morro de São João Alkaline Complex, modified from Fagundes (2020); D. Geological map of Cabo Frio Island, modified from Sichel et al. (2008).

The $^{40}K/^{40}Ar$ geochronological data show ages of *ca*. 50 Ma and 52.6 ± 2.0 Ma for whole-rock tinguaites (phonolites), 54.0 ± 2.6 Ma for biotite from pulaskite, and 72.4 ± 2.9 Ma for alkali feldspar from tinguaite (Amaral et al., 1967, recalculated by Sonoki & Garda, 1988). The $^{40}Ar/^{39}Ar$ data yielded an age of 54.83 ± 0.35 Ma for biotite crystal from nepheline syenite (Motoki et al., 2013). Refer to the Supplementary Material for further details on the geochronological data.

4.2 New Geochronological Data

This study contributes to the understanding of the PCCFA by providing new geochronological data (U-Pb and $^{40}Ar/^{39}Ar$) for the Itatiaia, Tinguá, and Morro dos Gatos massifs. The new ages are presented in the same order as in the previous section, from west to east, starting with the results from the U-Pb method and subsequently, where available, the data from the $^{40}Ar/^{39}Ar$ method. In addition to these data, the petrographic analysis results of the studied samples by U-Pb are also presented. All these ages, along with important information, are summarized in Table 3. For more detailed data of these ages, as well as to review the zircons analyzed using the U-Pb method, see the Supplementary Material.

For the Itatiaia massif, a sample of syenite (ITA 30A; Figure 6A) was studied using the U-Pb method. This rock is medium to coarse-grained, has inequigranular texture, and contains subhedral to anhedral crystals of perthitic feldspar, hornblende, and aegirine (Figure 6B). Minor minerals include biotite, titanite, and quartz, while zircon, apatite, and opaque minerals are identified as accessory minerals. The U-Pb analyses of the zircons yielded an age of 70.2 ± 2.7 Ma (MSWD = 0.2; P = 0.65 – Figure 6C).

Table 3 Summary table of the ages presented in this study for the Itatiaia, Tinguá, and Morro dos Gatos complexes, obtained using U-Pb and $^{40}Ar/^{39}Ar$ methods.

Complex	Method	Age (Ma)	Rock	Comment
Itatiaia	U-Pb	70.2 ± 2.7	Syenite	27 zircon grains were analyzed, and 18 grains were used to obtain the age
	$^{40}Ar/^{39}Ar$	67.31 ± 0.78	Nepheline syenite	Biotite grains were analyzed
Tinguá	U-Pb	69.3 ± 2.2	Nepheline syenite	27 zircon grains were analyzed, and 18 grains were used to obtain the age
	$^{40}Ar/^{39}Ar$	71.55 ± 0.49	Syenite	Hornblende grains were analyzed
Morro dos Gatos	U-Pb	65.4 ± 2	Monzonite	18 zircon grains were analyzed, and 8 grains were used to obtain the age

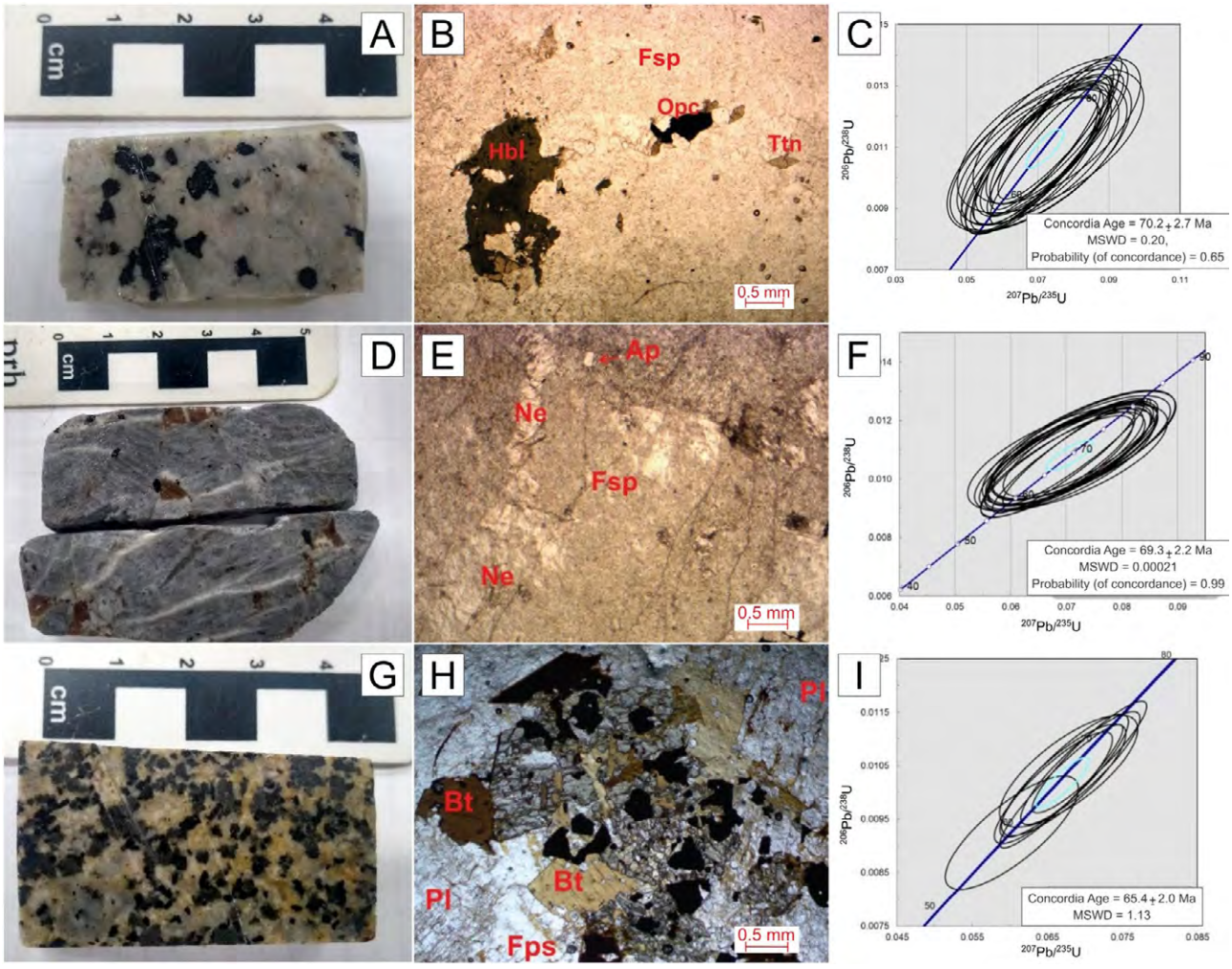

Figure 6 A-C. Itatiaia Massif; A. Photograph of the sample analyzed by U-Pb; B. Photomicrograph of the sample showing the presence of alkali feldspar (fsp) associated with hornblende (hbl), titanite (ttn), and opaque minerals (opc); C. U-Pb Concordia age diagram of zircon crystals from Itatiaia Massif; D-F. Tinguá Massif; D. Photograph of the sample analyzed by U-Pb; E. Photomicrograph of the sample showing the presence of alkali feldspar and nepheline (ne) associated with apatite (ap); F. U-Pb Concordia age diagram of zircon crystals from Tinguá Massif; G-I. Morro dos Gatos Alkaline Hill; G. Photograph of the sample analyzed by U-Pb; H. Photomicrograph of the sample showing the presence of alkali feldspar, plagioclase (pl), biotite (bt), and opaque minerals; I. U-Pb Concordia age diagram of zircon crystals from Morro dos Gatos Alkaline Hill.

The $^{40}Ar/^{39}Ar$ analysis was performed on biotite crystals from a biotite- and amphibole-bearing nepheline syenite sample (ITA 22A). This study obtained an age of 67.31 ± 0.78 Ma (MSWD = 1.5 – Figure 7A), slightly younger than the age determined by U-Pb. Compared to previously conducted geochronological analyses, the obtained ages for Itatiaia Complex fall within the same range, indicating consistency between the studies.

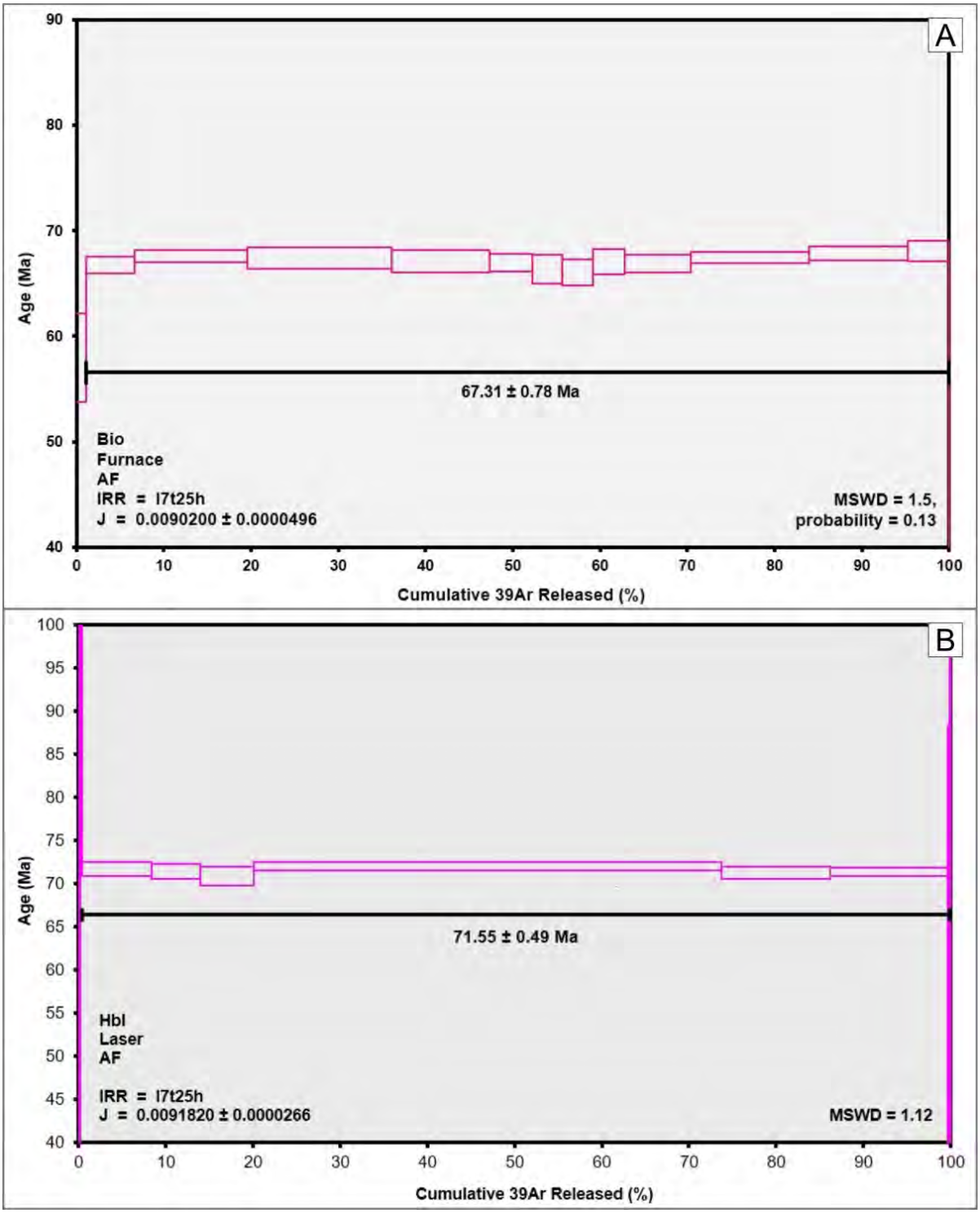

Figure 7 $^{40}Ar/^{39}Ar$ step-heating diagram: A. Biotite of the Itatiaia massif; B. Hornblende crystal from the Tinguá massif.

For the Tinguá massif, a nepheline syenite sample (TIG 04E; Figure 6D) medium- to coarse-grained and with gray color was studied using the U-Pb method. The rock is inequigranular and comprises subhedral to anhedral crystals of perthitic feldspar and nepheline (Figure 6E). Minor minerals include hornblende and aegirine, while accessory minerals include titanite, opaque, zircon, and apatite. The U-Pb results yielded an age of 69.3 ± 2.2 Ma (MSWD = 0.00021 – Figure 6F).

The $^{40}Ar/^{39}Ar$ study was conducted on hornblende crystals obtained from an amphibole- and biotite-bearing syenite (TIG-01). The analysis yielded an age of 71.55 ± 0.49 Ma (MSWD = 1.12 – Figure 7B), slightly older than the first age. When compared to previous studies, all the newly presented ages are older, suggesting that the massif formed earlier than previously known (*ca.* 3.5 Ma), primarily due to the Ar-Ar result.

Finally, a monzonite sample (MDG 03B; Figure 6G) with coarse-grained and equigranular texture and mesocratic feature was selected for the Morro dos Gatos massif. The rock predominantly comprises plagioclase, K-feldspar, biotite, and clinopyroxene, with quartz, apatite, and opaque minerals as accessory minerals (Figure 6H). The U-Pb analysis of zircons from this sample provided an age of 65.4 ± 2 Ma (MSWD = 1.13 – Figure 6I), marking the first age determination for this massif.

4.3 Lithogeochemistry

The lithogeochemical data gathered in this study are fully presented in the Supplementary Material. The total lithogeochemical results by lithology for each complex, along with classifications based on information provided by previous studies, are summarized in Table 4. However, to ensure the quality of the information, a filter was applied to the results when compared to the SiO_2 content. In these cases, samples were selected in which the oxides Na_2O and K_2O, in addition to silica, were not missing, and the total sum of the analyses was above 97%.

From various diagrams (Figures 8, 9 and 10), it can be observed that silica can be used to categorize rocks into two broad groups: 1) those with lower silica content (ranging from ca. 35 wt.% – to 50 wt.%); 2) those with higher silica content (ranging from 50 wt.% to *ca.* 75 wt.%). The less evolved rocks are associated with leucitite, tephrite, and basanite (Poços de Caldas Massif), and the more evolved ones are syenites and phonolites (Guarino et al., 2021). Some rocks from the Itatiaia Massif exhibit high silica contents and can be classified as silica-oversaturated (Rosa & Ruberti, 2018).

Table 4 Number of lithogeochemical samples classified by lithology for the PCCFA complexes. The samples classified in this table as "not defined" are associated with those presented as acronyms by the authors, which could not be directly categorized, and with results in which the samples were not classified individually. See the Supplementary Material for result details.

Rock/Lithotype	Complexes								
	Poços de Caldas	Itatiaia	Morro Redondo	Mendanha	Tanguá	Rio Bonito	Soarinho	Morro de São João	Cabo Frio Island
Nepheline syenite	49	37	12	0	0	0	0	2	22
Alkaline syenite	0	0	0	0	0	0	0	0	7
Quartz syenite	0	29	0	0	0	0	0	0	0
Phonolite	62	0	2	0	0	0	0	0	17
Monzonite	0	1	0	0	0	0	0	0	0
Lamprophyre	2	0	0	0	0	0	0	0	0
Leucitite	8	0	0	0	0	0	0	0	0
Tephrite	9	0	0	0	0	0	0	0	0
Basanite	3	0	0	0	0	0	0	0	0
Foidite	0	4	0	0	0	0	0	0	0
Mafurite	0	1	0	0	0	0	0	0	0
Trachyte	0	4	4	0	0	0	0	0	7
Melagabbro	0	1	0	0	0	0	0	0	0
Not Defined	0	5	6	10	16	23	16	13	11
Total Complex	133	82	24	10	16	23	16	15	64

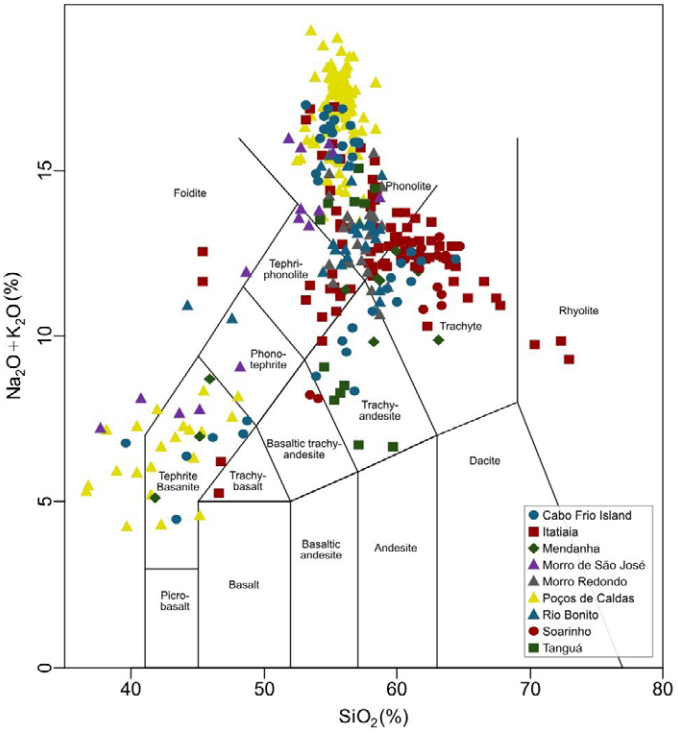

Figure 8 TAS diagram (Total alkali versus SiO2) by Le Bas et al. (1986) for the major PCCFA alkaline complexes. Data from Araújo (1995), Guarino et al. (2021), Mota (2012), Motoki et al. (2013; 2015), Rosa & Ruberti (2018), and Schorscher & Shea (1992).

In the TAS diagram (Figure 8) the less evolved samples predominantly plot within the tephrite/basanite or foidite fields, with a smaller number in the phono-tephrite, trachy-basalt, and basalt fields. Notably, these rocks, particularly those associated with the Poços de Caldas Complex, exhibit a positive correlation. On the other hand, the more evolved rocks are primarily classified as phonolite or trachyte, with some classified as tephri-phonolite, trachy-andesite, basaltic trachy-andesite, or rhyolite. A distinguishing feature of these silica-rich samples is that some rocks show positive correlations (e.g., Cabo Frio Island, between trachy-andesite and trachyte), but overall, most samples display a negative correlation. Another notable observation is a clear gap between the less evolved and more evolved rocks, with no intermediate results.

In the Harker diagrams for major elements (Figure 9), several correlations (mostly negatives) are observed compared to silica content. The Harker diagrams for TiO_2 and CaO show a negative correlation, with the less evolved rocks having a more vertical slope. For the Al_2O_3 diagram, the silica-depleted rocks exhibit a positive correlation, while the silica-enriched ones show a negative correlation. However, any interpretation of this behavior, along with the data dispersion for Na_2O and K_2O, should be approached cautiously because these oxides can be heavily influenced by the weathering of these rocks. Figure 10 presents Harker diagrams for trace elements relative to silica. In this case, in addition to the previously mentioned filter, trace element analyses with concentrations significantly higher than the others (possible outliers) were excluded to avoid distorting the data's overall trends (see the Supplementary Material for the complete data). These results show a slight negative correlation in the less evolved rocks from Poços de Caldas for elements such as Rb, Sr, Zr, Y, and Nb. The data are more scattered for the more evolved rocks, but positive correlations can still be noted for Rb and Nb in the Itatiaia rocks.

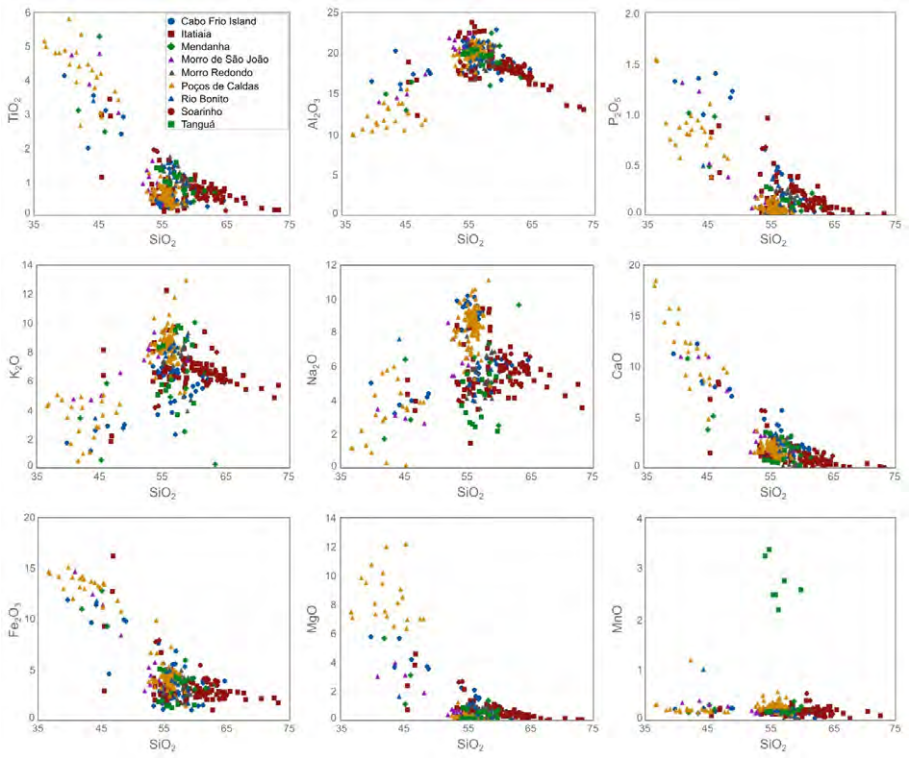

Figure 9 Harker diagram for major elements (wt%) for the major PCCFA alkaline complexes. Data from Araújo (1995), Guarino et al. (2021), Mota (2012), Motoki et al. (2013; 2015), Rosa & Ruberti (2018), and Schorscher & Shea (1992).

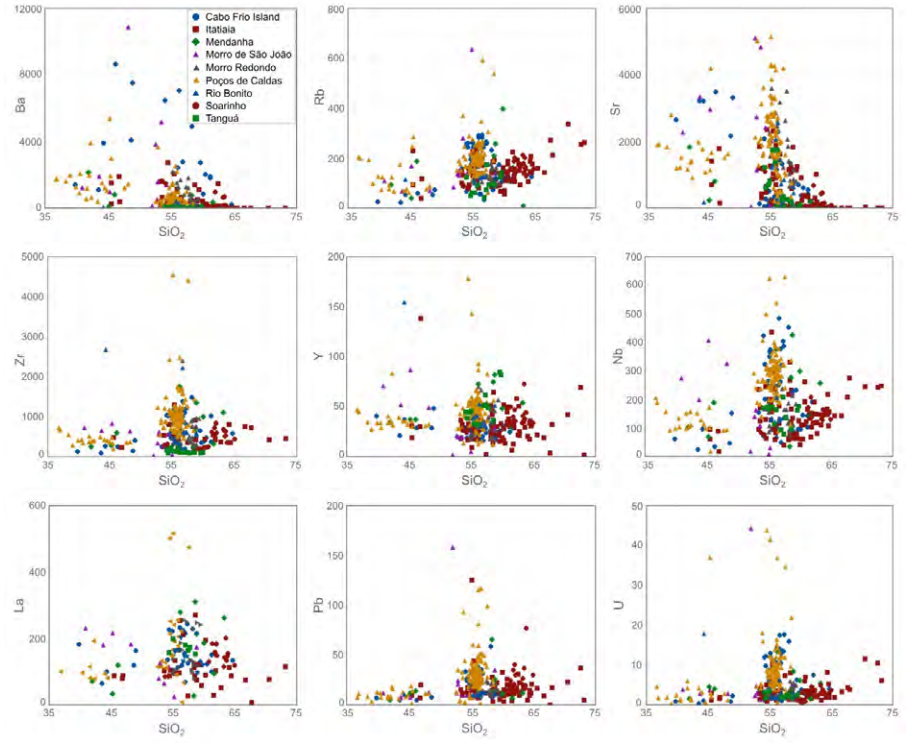

Figure 10 Harker diagram for trace elements (ppm) for the major PCCFA alkaline complexes. Data from Araújo (1995), Guarino et al. (2021), Mota (2012), Motoki et al. (2013; 2015), Rosa & Ruberti (2018), and Schorscher & Shea (1992).

The normalized diagrams (Figures 11 and 12) are presented by complex, and in some cases, the results are divided into two figures to facilitate visualization. Additionally, the data are presented as ranges, showing the maximum and minimum values found for each lithology within each complex. This approach allows for clear observation of the variations in results reported in previous studies.

The trace elements normalized to the primitive mantle (McDonough & Sun, 1995) reveal negative anomalies for Ba, Sr, P, and Ti in the more evolved rocks (Figure 11). Positive anomalies are less frequent and are associated with Rb, Ba, Sr, Pb, and Zr. Certain elements show significant differences in the normalized data across lithotypes, such as Ba and Sr in the three lithotypes of the Itatiaia Complex, Ba in the nepheline syenite and phonolite, and Pb in the phonolite, both in the Poços de Caldas Complex. The less evolved rocks (lines – Figure 11B) exhibit low variation in element content, with notable U and Pb anomalies.

The REE normalized to the primitive mantle (McDonough & Sun, 1995 – Figure 12) indicate that all complexes are characterized by an enrichment in light REE (La_N/Yb_N = 5.0 – 230.2 and La_N/Sm_N = 2.4 – 450.3). The heavy REE display distinct descending or ascending patterns, regardless of the specific alkaline complex. The Eu anomaly is the most prevalent and is be observed in nearly all complexes, with either negative or positive behavior in the more evolved rocks. Both the presence (negative and/or positive) and absence of the Eu anomaly can be observed within a single lithology of a single massif, such as in the nepheline syenites from the Cabo Frio Island, Itatiaia, Morro Redondo, and Rio Bonito complexes (see Supplementary Material). Significant differences in minimum and maximum values are also observed for certain lithotypes, such as the nepheline syenite and phonolite from the Poços de Caldas Complex, as well as among the different lithologies of the Itatiaia and Rio Bonito complexes. The less evolved rocks (lines – Figure 12B) show less variation in REE content, and Eu anomalies are rare.

4.4 Isotopic Geochemistry

The compiled isotopic geochemistry data are provided in the Supplementary Material. Table 5 summarizes the data collected in this study, showing the number of isotope results per massif, along with their minimum and maximum values. Figure 13 presents a boxplot diagram of the analyses performed for the massifs. It can be observed that the $^{87}Sr/^{86}Sr_{(i)}$ ratios for the Mendanha and Tanguá complexes show the greatest variability, unlike the more consistent behavior of the other massifs. In contrast, the Morro Redondo, Poços de Caldas, and Morro de São João complexes are the only that display results classified as outliers. The largest variations for the $^{143}Nd/^{144}Nd_{(i)}$ ratios are associated with the Mendanha, Itatiaia, and Poços de Caldas complexes. At the same time, the smallest range is found in the Morro de São João and Morro Redondo complexes.

According to Thompson et al. (1998), the Poços de Caldas alkaline massif has $^{87}Sr/^{86}Sr_{(i)}$ ratios from 0.70474 to 0.70487, $^{143}Nd/^{144}Nd_{(i)}$ ratios from 0.51243 to 0.51246, and ε_{Nd} from - 2.14 to - 1.43. Additionally, Guarino et al. (2021) studied different lithotypes and found that the nepheline syenites have $^{87}Sr/^{86}Sr_{(i)}$ ratios ranging between 0.70503 and 0.70540, and ε_{Nd} between - 3.9 and - 2.5; the phonolites have $^{87}Sr/^{86}Sr_{(i)}$ data varying from 0.70511 to 0.70527 and ε_{Nd} from - 3.4 to - 3.2; and basic-ultrabasic lavas have slightly less radiogenic $^{87}Sr/^{86}Sr_{(i)}$ ratios, ranging from 0.70440 to 0.70498 and ε_{Nd} from - 3.7 to - 1.2.

Rosa (2017) indicated that the Itatiaia Complex rocks have $^{87}Sr/^{86}Sr_{(i)}$ ratios ranging from 0.70469 to 0.70503 for the S-SE sector and 0.70533 and 0.70643 for the S-C and S-NW sectors, respectively. The $^{143}Nd/^{144}Nd_{(i)}$ ratios vary from 0.512409 to 0.512362 for the S-SE sector, while for the S-C and S-NW sectors, the values range from 0.512329 to 0.512223. The Morro Redondo Complex has $^{87}Sr/^{86}Sr_{(i)}$ ratios ranging from 0.70565 to 0.71042 and $^{143}Nd/^{144}Nd_{(i)}$ from 0.51234 to 0.51240 (Mota, 2012). For the Mendanha Complex, this last author indicated that the $^{87}Sr/^{86}Sr_{(i)}$ ratios vary between 0.70514 and 0.72347, $^{143}Nd/^{144}Nd_{(i)}$ ranges from 0.512180 to 0.512445, and ε_{Nd} varies between - 8.99 and - 3.77. The dikes of the Mendanha Complex have $^{87}Sr/^{86}Sr_{(i)}$ ratios ranging from 0.70455 to 0.70820, $^{143}Nd/^{144}Nd_{(i)}$ from 0.51250 to 0.51255, and ε_{Nd} from - 0.85 to - 0.07 (Thompson et al., 1998).

The Tanguá massif has a $^{87}Sr/^{86}Sr_{(i)}$ ratio of 0.7062 (Motoki et al., 2010; Sichel et al., 2012), more radiogenic than Soarinho dikes, which have $^{87}Sr/^{86}Sr_{(i)}$ ratios of 0.70484 and 0.70494, $^{143}Nd/^{144}Nd_{(i)}$ ratios of 0.51247 and 0.51241, and ε_{Nd} of - 1.60 and - 2.86 (Thompson et al., 1998). For MSJ, moderate radiogenic ratios were obtained for the $^{87}Sr/^{86}Sr_{(i)}$ ratio (between 0.7049 and 0.7061) and low for $^{143}Nd/^{144}Nd_{(i)}$ (between 0.512361 and 0.512428). The ε_{Nd} values vary between - 4.03 and - 5.54 (Mota et al., 2009). The Cabo Frio dikes have $^{87}Sr/^{86}Sr_{(i)}$ ratios varying from 0.70404 to 0.70460, $^{143}Nd/^{144}Nd_{(i)}$ from 0.51239 to 0.51247, and ε_{Nd} from - 3.56 to - 1.90 (Thompson et al., 1998).

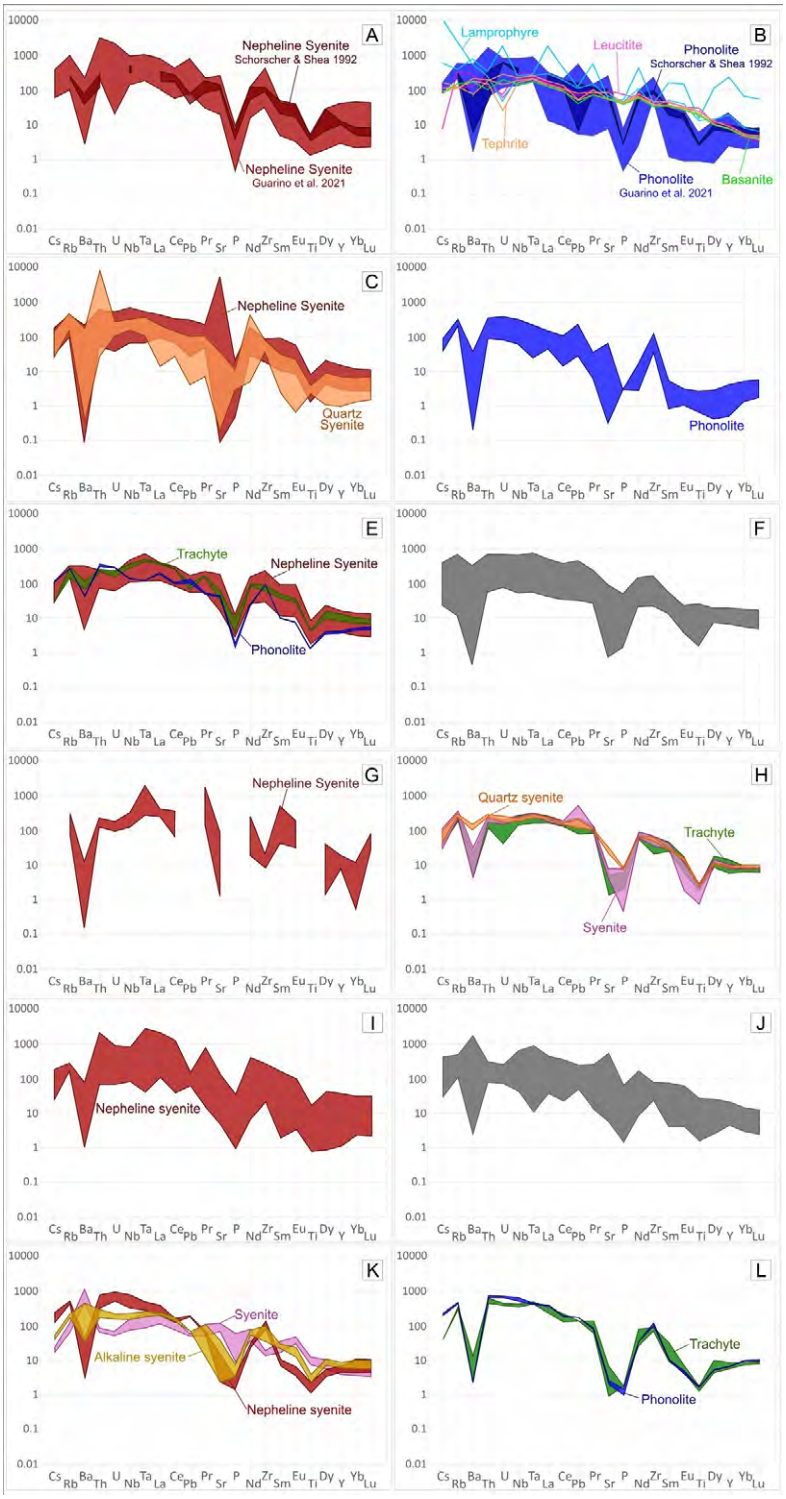

Figure 11 Primitive mantle-normalized trace elements (McDonough and Sun, 1995) for the main PCCFA alkaline complexes: A-B. Poços de Caldas Complex; C-D. Itatiaia Complex; E. Morro Redondo Complex; F. Mendanha Complex. Mota (2012) did not classify the samples by lithotypes but studied syenites, trachytes, breccias, and lamprophyre dikes; G. Tanguá Complex; H. Soarinho Complex; I. Rio Bonito Complex; J. Morro do São João Complex. Mota (2012) did not classify the samples by lithotypes but studied syenites, malignite, shonkinite, and gabbro; K-L. Cabo Frio Complex. The geochemical data are from Guarino et al. (2021), Mota (2012), Motoki et al. (2015), Rosa (2017), Schorscher & Shea (1992), and Silva (2019).

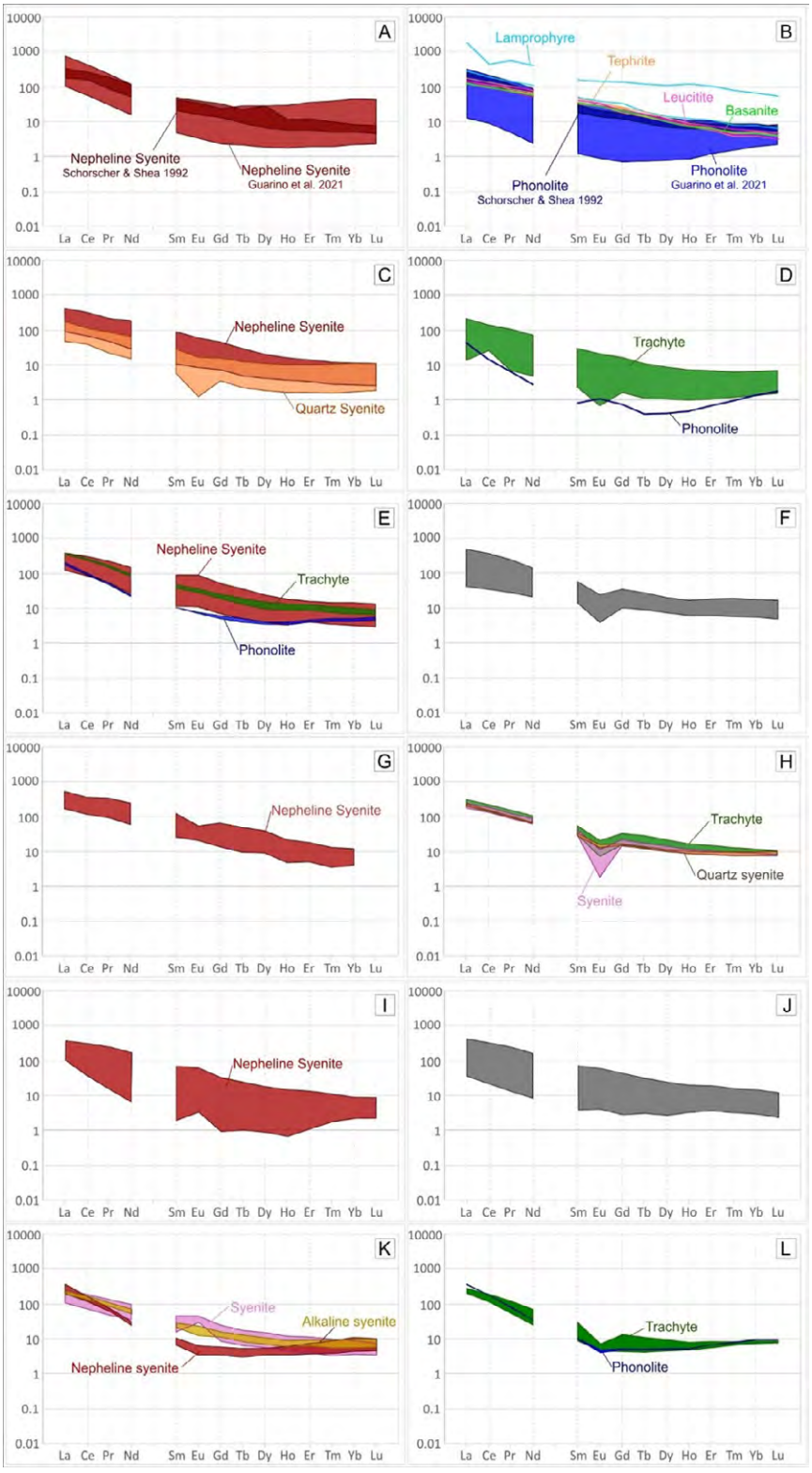

Figure 12 Primitive mantle-normalized rare earth elements (McDonough & Sun, 1995) for the main PCCFA alkaline complexes: A-B. Poços de Caldas Complex; C-D. Itatiaia Complex; E. Morro Redondo Complex; F. Mendanha Complex; G. Tanguá Complex; H. Soarinho Complex; I. Rio Bonito Complex; J. Morro do São João Complex; and K-L. Cabo Frio Complex. The geochemical data are from Araújo (1995), Guarino et al. (2021), Mota (2012), Motoki et al. (2015), Rosa (2017), Schorscher & Shea (1992), and Silva (2019).

Table 5 Summary of isotopic ratios ($^{87}Sr/^{86}Sr_{(i)}$ e $^{143}Nd/^{144}Nd_{(i)}$) for different massifs of the PCCFA. The table presents the number of data points collected and the minimum and maximum values. The data were obtained from the works of Brotzu et al. (2007), Guarino et al. (2021), Mota (2012), Motoki et al. (2010), Rosa (2017), Sichel et al. (2012), Thompson et al. (1998), and Ulbrich et al. (2003).

Massif/Complex	$^{87}Sr/^{86}Sr_{(i)}$			$^{143}Nd/^{144}Nd_{(i)}$		
	Number	Minimum	Maximum	Number	Minimum	Maximum
Poços de Caldas	20	0.70443	0.70912	20	0.512360	0.512560
Itatiaia	14	0.70469	0.70643	18	0.512223	0.512560
Morro Redondo	9	0.70565	0.71042	9	0.512344	0.512400
Mendanha	12	0.70471	0.72347	14	0.512177	0.512600
Morro do São João	15	0.70490	0.70985	15	0.512333	0.512428
Soarinho	2	0.70492	0.70498	2	0.512460	0.512510
Tanguá	4	0.70620	0.71280	0	–	–
Rio Bonito	4	0.70510	0.70520	0	–	–
Cabo Frio	4	0.70419	0.70490	3	0.512420	0.512500

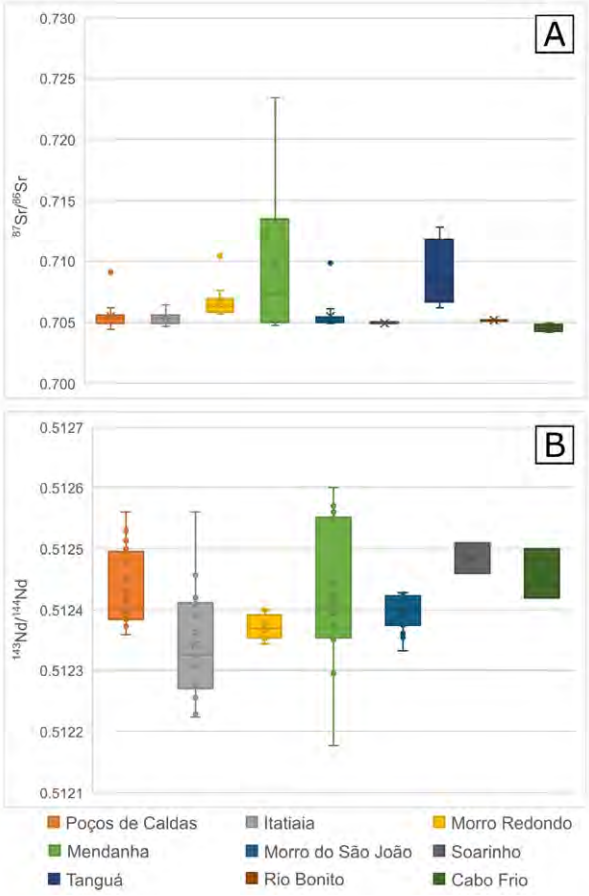

Figure 13 Boxplot showing the variation in isotopic ratios ($^{87}Sr/^{86}Sr_{(i)}$ and $^{143}Nd/^{144}Nd_{(i)}$) for different massifs of the PCCFA. The data were obtained from the works of Brotzu et al. (2007), Guarino et al. (2021), Mota (2012), Motoki et al. (2010), Rosa (2017), Sichel et al. (2012), Thompson et al. (1998), and Ulbrich et al. (2003).

5 Discussion

The PCCFA Alkaline Province mainly comprises nepheline syenites, syenites, phonolites, and trachytes. Guarino et al. (2019) suggest that the similarity between the massifs of this alignment in terms of major and trace elements may indicate mantle sources that are similar both geochemically and isotopically. The occurrence of less evolved rocks (leucitite, tephrite, and basanite) and more evolved ones (syenites, phonolites, and trachytes) in the same complex, such as Poços de Caldas, can be attributed to fractional crystallization processes, as suggested by Guarino et al. (2019). The most evolved rocks range from silica-undersaturated (nepheline syenite) to silica-supersaturated (quartz-syenite), which are associated with crustal contamination processes, allowing them to cross the thermal barrier, as observed in the Itatiaia and Soarinho complexes (e.g., Rosa, 2017 and Silva et al., 2023).

According to Motoki et al. (2015), several massifs have pyroclastic volcanic conduits, primarily filled with welded tuff breccia. These breccias, which are outcropped preferentially at the intrusion edges, are polymictic (containing massif and host-rock fragments) and may feature a syenitic matrix and compositional zoning of fragments (e.g., Mota, 2012, and Silva, 2019). The increasing content of alkaline rock fragments closer to the intrusion suggests that some pulses intruded into coller alkaline rock, brecciating it.

Correlations between silica and oxides, such as TiO_2, and P_2O_5, may indicate the mineral fractionation of rocks, such as titanite and apatite. This further supported by trace element anomalies, such as Ba, Sr, Rb, and Zr. The same lithology within a massif can exhibit a wide range of values in normalized diagrams (Figures 11 and 12), suggesting that the rocks may have undergone different evolutionary processes during the formation of the complexes. Studies like those by Motoki et al. (2015) and Rosa (2017) suggest the presence of crustal assimilation processes during emplacement, which could account for these variations. Additionally, the Eu anomaly is associated with europium's ability to replace Ca, indicating fractionation into plagioclase and suggesting distinct REDOX conditions in the magma crystallization. Hence, the presence of positive and negative anomalies in the PCCFA massifs (or even the absence of anomalies), within the same complex and lithology, reinforce the idea of changing conditions and plagioclase fractionation during the massif evolution (see Eu/Eu* in the Supplementary Material). For the slight compositional difference of less evolved rocks (normalized data) indicates similar sources and petrogenetic processes as suggested, as noted by Guarino et al. (2021). Additionally, the U and Pb anomalies may indicate zircon fractionation, while the absence of the Eu anomaly suggests that plagioclase fractionation did not occur during the formation of these rocks.

Sr- and Nd-isotopic data from the PCCFA complexes show close ranges, with trends between DMM and EM1 or DMM and EM2 (Figure 14), suggesting pre-eruptive isotopic homogeneity and a source mixture. Some authors have linked the genesis of these massifs to the context of a broad lithospheric mantle (e.g., Riccomini et al., 2005; Guarino et al., 2021; and Ulbrich et al., 2003), an enriched mantle (e.g., Silva, 2019), or even a variable contribution of both depleted and enriched sources (Gordon et al., 2023). Guarino et al. (2021) demonstrated that the difference observed for the Sr-Nd isotopic composition within the PCCFA is associated with a lithospheric mantle rich in highly potassium-metasomatized liquid.

According to Willbold & Stracke (2010 and references therein), different continental crust types may be involved with magma generation from sources classified as Enriched Mantle (EM). Using Eu/Eu* and $^{87}Sr/^{86}Sr$ data, it is possible to infer the participation of either lower or upper continental crust. The authors argued that the involvement of crustal sediments associated with the oceanic crust plays a significant role in the formation of these enriched sources. This view is supported by Rosa (2017), who, based on Sr-Nd-Pb isotopic signatures, described a normal mantle from which melting influenced crustal contamination during its evolution.

Although some authors emphasize that the PCCFA rocks are not cogenetic and not linked to mantle plumes (e.g., Riccomini et al., 2005; Guarino et al., 2021), certain features – such as possible decrease in age towards the east and specific isotopic signatures - may indicate a plume-related origin (Thompson et al., 1998). Tomographic data reveal a potential correlation between onshore and offshore structures linked with shallow mantle plumes, further supporting this last model (Celli et al., 2020). Regardless of the model, the structural control of magmatism in the South American alkaline provinces is evident. The relationship of these preexisting structures with the magmatic intrusions is supported by the dikes' and massifs' orientation and reinforced by similar structural fracture zones in the onshore and offshore contexts (Riccomini et al, 2005; Santos & Hackspacher, 2021).

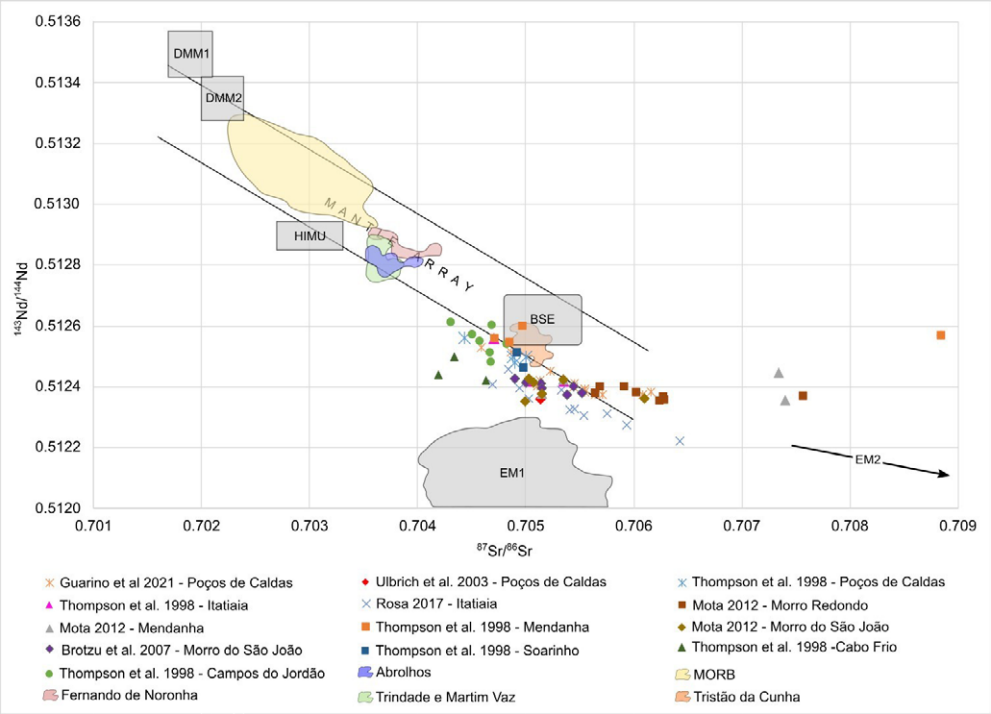

Figure 14 $^{143}Nd/^{144}Nd$ versus $^{87}Sr/^{86}Sr$ diagram of PCCFA alkaline complexes, modified from Mota (2012).

Based on previous and new geochronological data, certain characteristics of the PCCFA genesis can be identified. The new U-Pb (70.2 ± 2.7 Ma) and $^{40}Ar/^{39}Ar$ (67.31 ± 0.78 Ma) ages of the Itatiaia massif fall within the intermediate range of previously published ones. On the other hand, the new ages obtained for the Tinguá massif by the U-Pb (69.3 ± 2.2 Ma) and $^{40}Ar/^{39}Ar$ (71.55 ± 0.49 Ma) methods are the oldest yet identified for the complex. Since U-Pb (Figure 3B) and $^{40}Ar/^{39}Ar$ (Figure 3C) data are still more restricted, $^{40}K/^{40}Ar$ results (Figure 3A) for a few samples were also used to complement the interpretations. These methods data of some massifs were combined in Figure 15A, which used previously published ages and new ones for several massifs (Poços de Caldas, Passa Quatro, Itatiaia, Tinguá, Tanguá, Soarinho, and Cabo Frio). Additionally, an aerial satellite image (Figure 15B), and a topographic profile (Figure 15C) display the distances between these massifs. The data show a possible age-decreasing trend (Figure 15A) from west (Poços de Caldas Complex) to east (Cabo Frio Complex), consistent with the stationary plume model (Thompson et al., 1998; and Thomaz Filho et al., 2005). However, some ages highlight the non-regressive age concept.

The Itatiaia and Tinguá complexes, located in the central portion of the alignment, show the oldest (90.5 ± 2.2 Ma) and youngest (39.1 ± 3.4 Ma) PCCFA ages published, respectively. Besides that, some Poços de Caldas Complex ages are contemporaneous with those of the Cabo Frio Complex, respectively the westernmost and easternmost massifs of the alignment. When considering only the U-Pb and $^{40}Ar/^{39}Ar$ ages (Figure 3), which are more precise and recent, contemporaneous results are observed for the Tinguá, Mendanha, Tanguá, Rio Bonito, Morro dos Gatos, and Morro do São João complexes (from west to east).

In summary, the geochronological data suggest no clear pattern of gradual decrease in age towards the eastern region, and massifs in different geographic locations may exhibit contemporaneous ages. The geochronological data variability for the same massif reinforces the presence of different pulses during the complexes' emplacement, as suggested by Rosa & Ruberti (2018).

These geochronological characteristics imply that the PCCFA genesis cannot be associated with a conventional mantle plume (e.g., Hawaii hotspot), with an evolution from west to east. An alternative hypothesis involves an unconventional plume that splits into distinct conduits, dividing in different directions, as suggested by Courtillot et al. (2003) and Tsekhmistrenko et al. (2021). These diffuse intrusions may have taken advantage of pre-existing structures to reach the surface, which could explain the observed age distribution and structural orientations. However, further studies are required to confirm that this new concept applies to the PCCFA, and this indication should be taken as a suggestion for further works.

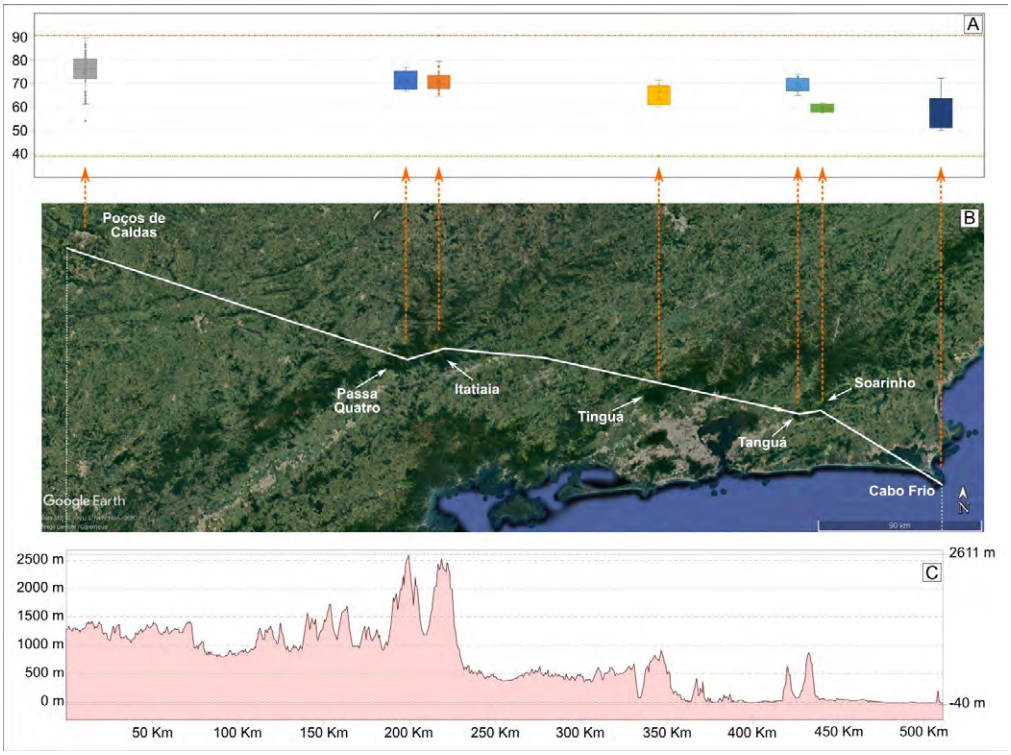

Figure 15 Image comparing the ages of some PPCFA complexes, with the geographic positioning and topographic profile: A. The geochronological data were obtained by the $^{40}K/^{40}Ar$, U-Pb and $^{40}Ar/^{39}Ar$ based on the following works: Amaral et al. (1967); Biondi (2005); Brotzu et al. (1989); Brotzu et al. (1992); Bushee (1971); Deckart et al. (1998); Ferrari (2001); Montes-Lauar and Pacca (1988); Montes-Lauar et al. (1995); Mota (2012); Motoki et al. (2013); Ribeiro Filho & Cordani (1966); Shea (1992); Silva (2019); Silva et al. (2020, 2023); Sonoki & Garda (1988); Takenaka (2014); Thompson et al. (1998); Ulbrich et al. (2002); Vlach et al. (2003); and the present study; B. The geographical position of the selected complexes to indicate the distance between them and the position in the PCCFA context; C. Topographic profile evolution, from the Poços de Caldas Complex to the Cabo Frio Complex. B and C from Google Earth Pro.

6 Concluding Remarks

1. The PCCFA massifs have similar lithotypes, predominantly comprising nepheline syenites, syenites, phonolites, and trachytes, which are generally silica-undersaturated. However, some massifs are also composed of less evolved rocks, which present low chemical variability, suggesting similar sources and petrogenetic processes. The presence of silica-oversaturated rocks in the Itatiaia and Soarinho massifs may be linked to crustal contamination, indicating that the magma crossed the thermal barrier. This is reinforced by Sr-Nd-Pb isotopic signatures. The Eu anomalies for more evolved rocks suggest distinct REDOX conditions and different plagioclase fractionation behavior during the magma rise and the complexes' genesis, which is not observed in the less evolved rocks.
2. Isotopic data indicate a possible mixing of DMM and EM1 magma sources or DMM and EM2. The involvement of metasomatized rocks and crustal sediments is also associated with the genesis of the complexes' magma.
3. The new Tinguá massif ages (69.3 ± 2.2 Ma by U-Pb and 71.55 ± 0.49 Ma by $^{40}Ar/^{39}Ar$) indicated that it is older than previously thought. The Itatiaia geochronological data (70.2 ± 2.7 Ma by U-Pb and 67.31 ± 0.78 Ma by $^{40}Ar/^{39}Ar$) are consistent with earlier findings. Additionally, the first published age data for the Morro dos Gatos massif (65.4 ± 2 Ma using the U-Pb method) suggest a contemporaneous genesis with other massifs.
4. Although the geochronological data trend decreases gradually towards the east, the overall distribution indicates that the conventional stationary plume model may not fully explain the alignment genesis. A hypothesis for the first model is the presence of a mantle plume with distinct conduits, which used these regional structures for the massif emplacement, reinforcing the importance of these structures. However, further studies are required to confirm this suggestion for PCCFA genesis.

7 Acknowledgments

This work was supported by CNPq (ProTrindade Program) [Process number. 557146/2009-7]; the MCT/CNPq project [number 26/2009]; and FAPERJ [Entidades Estaduais 2018 number 210.297/2018; APQ1 2019 number 210.179/2019; JCNE 2022 number 201.469/2022]. The corresponding author thanks Rio de Janeiro State University for supporting and encouraging his research and FAPERJ for the doctoral fellowship. MSc. Marco Aurélio Maia Teodoro thanks Prof. Dr. Anderson and Prof. Dr. Luiz Bertolino for all the teaching, support, and suggestions during this work. All authors thank the journal's editors and reviewers.

8 References

Almeida, F.F.M. 1983, 'Relações tectônicas das rochas alcalinas Mesozóicas da região meridional da Plataforma Sul-Americana', *Revista Brasileira de Geociências* vol. 13, pp. 139-58.

Almeida, F.F.M. 1991, 'O alinhamento magmático de Cabo Frio', *Simpósio de Geologia Do Sudeste*, vol. 2, pp. 423-8.

Amaral, G., Bushee, J., Cordani, U.G., Kawashita, K. & Reynolds, J.H. 1967, 'Potassium-argon ages of alkaline rocks from southern Brazil', *Geochim Cosmochim Acta*, vol. 31, 117-42.

Araújo, A.L. 1995, 'Geologia, geoquímica e petrologia das rochas alcalinas da ilha do Cabo Frio e das áreas continentais adjacentes, Arraial do Cabo-RJ', Masther´s thesis, Universidade Federal Fluminense, Niterói.

Biondi, J.C. 2005, 'Brazilian mineral deposits associated with alkaline and alkaline-carbonatite complexes. Mesozoic to Cenozoic Alkaline Magmatism in the Brazilian Platform', *FAPESP*, pp. 707-50.

Brotzu, P., Barbieri, M., Beccaluva, L., Garbarino, C., Gomes, C.B., Macciotta, G., Melluso, L., Morbidelli, L., Ruberti, E. & Sigolo, J.B. 1992, 'Petrology and geochemistry of the Passa Quatro alkaline complex, southeastern Brazil', *Journal of South America Earth Sciences*, vol. 6, pp. 237-52.

Brotzu, P., Beccaluva, L., Conte, A.M., Fonseca, M., Garbarino, C., Gomes, C.B., Leong, R., Macciotta, G., Mansur, R.L., Melluso, L., Morbidelli, L., Ruberti, E., Sigolo, J.B., Traversa, G. & Valença, J.G. 1989, 'Petrological and Geochemical Studies of Alkaline Rocks from Continental Brazil: 8. The Syenitic Intrusion of Morro Redondo, RJ', *Geochimica Brasiliensi,* vol. 3, pp. 63-80.

Brotzu, P., Melluso, L., Bennio, L., Gomes, C.B., Lustrino, M., Morbidelli, L., Morra, V., Ruberti, E., Tassinari, C. & D'Antonio, M. 2007, 'Petrogenesis of the Early Cenozoic potassic alkaline complex of Morro de São João, southeastern Brazil', *Journal of South American Earth Sciences*, vol. 24, pp. 93-115.

Brotzu, P., Melluso, L., D'Amelio, F., Lustrino, M., Comin-Chiaramonti, P. & Gomes, C.B. 2005, 'Potassic dikes and intrusions of the Serra do Mar Igneous Province (SE Brazil)', in P. Comin-Chiaramonti & CB Gomes (eds), *Mesozoic to Cenozoic Alkaline Magmatism in the Brazilian Platform*, EDUSP/FAPESP, São Paulo, pp. 443-72.

Bushee, J. 1971, 'Geochronological and petrographic studies of alkaline rocks from Southern Brazil. I. Potassium-argon ages of some alkaline rocks from Southern Brazil. II. A geochronological study of the alkaline massif of Poços de Caldas, Brazil. III. Geology and petrogr', Unpublished PhD Thesis, 143p.

Celli, N. L., Lebedev, S., Schaeffer, A. J., Ravenna, M. & Gaina, C. 2020, 'The upper mantle beneath the South Atlantic Ocean, South America and Africa from waveform tomography with massive data sets', *Geophysical Journal International*, vol. 221, no. 1, pp. 178-204.

Chiessi, C.M. 2004, 'Tectônica cenozóica do Maciço Alcalino de Passa Quatro (SP-MG-RJ)', Dissertation, Universidade de São Paulo.

Cordani, U.G. & Teixeira, W. 1979, 'Comentários sobre as determinações geocronológicas existentes para as regiões das folhas Rio de Janeiro, Vitória e Iguape. Folhas Rio de Janeiro/Vitória (Iguapé SF23/24/SG 23)', in *Carta Geologica do Brasil ao Milionésimo-Texto explicativo*, DNPM, Brasília.

Courtillot, V., Davaille, A., Besse, J. & Stock, J. 2003, 'Three distinct types of hotspots in the Earth's mantle', *Earth and Planetary Science Letters*, vol. 205, pp. 295-308.

Deckart, K., Féraud, G., Marques, L.S. & Bertrand, H. 1998, 'New time constraints on dyke swarms related to the Paraná-Etendeka magmatic province, and subsequent South Atlantic opening, southeastern Brazil', *Journal of Volcanology and Geothermal Research*, vol. 80, pp. 67-83.

Dutra, C.V. 1966, 'Método chumbo-alfa e idades de zircões do maciço alcalino de Poços de Caldas, Minas Gerais', *Boletim do Instituto de Geologia*, vol. 1, no. 3-4.

Enrich, G.E.R., Azzone, R.G., Ruberti, E., Gomes, C.B. & Comin Chiaramonti, P. 2005, *Itatiaia, Passa Quatro and São Sebastião Island, the major alkaline syenitic complexes from the Serra do Mar region*, EDUSP/FAPESP, São Paulo.

Fagundes, M.B. 2020, 'Caracterização petrográfica e geoquímica do Complexo Alcalino do Morro de São João, Casimiro de Abreu-RJ', Master´s thesis, Universidade do Estado do Rio de Janeiro.

Ferrari, A.L. 2001, 'Evolução Tectônica do Graben da Guanabara', *Universidade de São Paulo*, vol. 1, 449.

Ferreira, L.C. 2018, 'Processamento, integração e interpretação de dados de aeromagnetometria e aerogamaespectrometria do estado do Rio de Janeiro', Universidade Federal Fluminense.

Geraldes, M.C., Motoki, A., Vargas, T., Iwanuch, W., Balmant, A. & Motoki, K.F. 2013, 'Geology, petrography and emplacement mode of the Morro dos Gatos Alkaline intrusive Complex, state of Rio de Janeiro, Brazil', *Geociências*, vol. 32, no. 4, pp. 625-39.

Gomes, C.B. & Comin-Chiaramonti, P. 2005, *An introduction to the alkaline and alkaline-carbonatitic magmatism in and around the Paraná Basin. Mesozoic to Cenozoic Alkaline Magmatism in the Brazilian Platform*, FAPESP, São Paulo.

Gordon, A.C., Santos, A.C., Caitano, G.R., Stanton, N. & Mohriak, W.U. 2023, 'Magmatic cycles in Santos Basin (SE Brazil): Geochemical characterization and magmatic sources', *Journal of South American Earth Sciences*, vol. 126, 104323.

Guarino, V., De' Gennaro, R., Melluso, L., Ruberti, E. & Azzone, R.G. 2019, 'The transition from miaskitic to agpaitic rocks, as highlighted by the accessory phase assemblages in the Passa quatro alkaline complex (Southeastern Brazil)', *The Canadian Mineralogist*, vol. 57, pp. 339-61.

Guarino, V., Lustrino, M., Zanetti, A., Tassinari, C.C.G., Ruberti, E., de' Gennaro, R. & Melluso, L. 2021, 'Mineralogy and geochemistry of a giant agpaitic magma reservoir: The Late Cretaceous Poços de Caldas potassic alkaline complex (SE Brazil)', *Lithos*, pp. 398-9, 106330.

Hackspacher, P.C. & Godoy, A.M. 1999. Vertical displacement during late-collisional escape tectonics (Brasiliano Orogeny) in the Ribeira Belt, São Paulo State, Brazil. *Journal of African Earth Sciences*, vol. 29, pp. 25-32.

Heilbron, M., Eirado, L.G. & Almeida, J. 2016, *Mapa geológico e de recursos minerais do estado do Rio de Janeiro*, CPRM.

Jackson, S.E., Pearson, N.J., Griffin, W.L. & Belousova, E.A. 2004, 'The application of laser ablation-inductively coupled plasma-mass spectrometry to in situ U–Pb zircon geochronology', *Chemical Geology*, vol. 211, no. 1-2, pp. 47-69.

Jourdan, F. & Renne, P.R. 2007, 'Age calibration of the Fish Canyon sanidine 40Ar/39Ar dating standard using primary K–Ar standards', *Geochimica et Cosmochimica Acta*, vol. 71, no. 2, pp. 387-402.

Koppers, A.A. 2002, 'ArArCALC – software for 40Ar/39Ar age calculations', *Computers & Geosciences*, vol. 28, no. 5, pp. 605-19.

Le Bas, M., Maitre, R. L., Streckeisen, A., Zanettin, B. & IUGS Subcommission on the Systematics of Igneous Rocks. 1986, 'A chemical classification of volcanic rocks based on the total alkali-silica diagram', *Journal of Petrology*, vol. 27, no. 3, pp. 745-50.

Le Maitre, R.W., Streckeisen, A., Zanettin, B., Le Bas, M.J., Bonin, B., Bateman, P., Bellieni, G., Dudek, A., Efremova, S., Keller, J., Lameyre, J.A., Sabine, P.A., Schmid, R., Sorensen, H. & Wooley, A.R. 2002, *Igneous rocks: A Classification and Glossary of Terms: Recommendations of the International Union of Geological Sciences Subcommission on the Systematics of Igneous Rocks, Cambridge University Press, Cambridge*, Cambridge University Press, Cambridge.

Macedo, B.N., Peternel, R., Santos, A.C.D. & Simas, M.P. 2022, 'Resende lamprophyres: New petrological and structural interpretations for a regional Upper Cretaceous alkaline mafic dyke swarm', *Brazilian Journal of Geology*, vol. 52, e20210043.

McDonough, W.F. & Sun, S.-S. 1995, 'The composition of the Earth', *Chemical Geology*, vol. 120, pp. 223-53.

Melluso, L., Guarino, V., Lustrino, M., Morra, V. & de'Gennaro, R. 2017, 'The REE- and HFSE-bearing phases in the Itatiaia alkaline complex (Brazil) and geochemical evolution of feldspar-rich felsic melts', *Mineralogical Magazine*, vol. 81, pp. 217-50.

Milani, E. J. 1997, 'Evolução tectono-estratigráfica da Bacia do Paraná e seu relacionamento com a geodinâmica fanerozóica do Gondwana sul-ocidental', PhD thesis, Universidade Federal do Rio Grande do Sul.

Monteiro, L.G.P. 2021, 'Petrogênese do Maciço Alcalino de Morro dos Gatos: implicações da tectônica do embasamento e seu potencial econômico', Final paper, Universidade do Estado do Rio de Janeiro.

Montes-Lauar, C.R., Pacca, I.G., Melfi, A.J. & Kawashita, K. 1995, 'Late Cretaceous alkaline complexes, southeastern Brazil: Paleomagnetism and geochronology', *Earth and Planetary Science Letters*, vol. 134, pp. 425-40.

Montes-Lauar, C.R. & Pacca, I.I.G. 1988, 'Estudo paleomagnético dos maciços alcalinos de Poços de Caldas, Passa Quatro e Itatiaia', Masther´s thesis, Universidade de São Paulo.

Mota, C.E.M. 2012, 'Petrogênese e geocronologia das intrusões alcalinas de Morro Redondo, Mendanha e Morro de São João: caracterização do magmatismo alcalino no estado do Rio de Janeiro e implicações geodinâmicas', PhD thesis, Universidade do Estado do Rio de Janeiro.

Mota, C.E.M., Geraldes, M.C., Horta De Almeida, J.C., Vargas, T., Marinho De Souza, D. & Pimentel Da Silva, A. 2009, 'Características Isotópicas (Nd e Sr), Geoquímicas e Petrográficas da Intrusão Alcalina do Morro de São João: Implicações Geodinâmicas e Sobre a Composição do Manto Sublitosférico', *Geologia USP: Série Científica*, vol. 9, no. 1.

Motoki, A., Araújo, A.L., Sichel, S.E., Geraldes, M.C., Jourdan, F., Motoki, K.F. & da Silva, S. 2013, 'Nepheline syenite magma differentiation with continental crustal assimilation for the Cabo Frio Island intrusive complex, State of Rio de Janeiro, Brazil', *Geociências*, vol. 32, pp. 195-218.

Motoki, A., Sichel, S.E., Soares, R., Aires, J.R., Savi, C., Petrakis, G.H. & Motoki, K.F. 2008, 'Rochas piroclásticas de preenchimento de condutos subvulcânicos do Mendanha, Itaúna e Ilha de Cabo Frio, RJ, e seu processo de formação com base no modelo de implosão de conduto', *Geociencias*, vol. 27, pp. 451-67.

Motoki, A., Sichel, S.E., Vargas, T., Aires, J.R., Iwanuch, W., Mello, S.L.M., Motoki, K.F., Da Silva, S., Balmant, A. & Gonçalves, J. 2010, 'Geochemical evolution of the felsic alkaline rocks of tanguá and Rio bonito intrusive bodies, state of Rio de Janeiro, Brazil', *Geociencias*, vol. 29, pp. 291-310.

Motoki, A., Sichel, S.E., Vargas, T., Melo, D.P. & Motoki, K.F. 2015, 'Geochemical behaviour of trace elements during fractional crystallization and crustal assimilation of the felsic alkaline magmas of the state of Rio de Janeiro, Brazil', *Anais Da Academia Brasileira De Ciências*, vol. 87, pp. 1959-79.

Netto, A.M., Geraldes, M.C. & Vignol-Lelarge, M.L. 2005, 'Idade traço de fissão em apatita do maciço alcalino do Medanha: implicações sobre o magmatismo cretáceo no Estado do Rio de Janeiro', *IX Simpósio de Geologia do Sudeste*.

Renne, P.R., Balco, G., Ludwig, K.R., Mundil, R. & Min, K. 2011, 'Response to the comment by WH Schwarz et al. on "Joint determination of 40K decay constants and 40Ar∗/40K for the Fish Canyon sanidine standard, and improved accuracy for 40Ar/39Ar geochronology" by PR Renne et al. (2010)', *Geochimica et Cosmochimica Acta*, vol. 75, no. 17, 5097-100.

Ribeiro Filho, E. & Cordani, U.G. 1966, 'Contemporaneidade das intrusões de rochas alcalinas do Itatiaia, Passa Quatro e Morro Redondo', *Repositório da Produção USP*, pp. 62-3.

Riccomini, C., Velázquez, V.F. & Gomes, C.B. 2005, 'Tectonic controls of the Mesozoic and Cenozoic alkaline magmatism in central-southeastern Brazilian Platform', in P. Comin-Chiaramonti & C.B. Gomes (eds), *Mesozoic to Cenozoic Alkaline Magmatism in the Brazilian Platform*, Edusp, São Paulo, pp. 31-56.

Rocha-Júnior, E.R.V., Marques, L.S., Babinski, M., Machado, F.B., Petronilho, L.A. & Nardy, A.J.R. 2020, 'A telltale signature of Archean lithospheric mantle in the Paraná continental flood basalts genesis', *Lithos*, vol. 364, 105519.

Rosa, P.A.S. & Ruberti, E. 2018, 'Nepheline syenites to syenites and granitic rocks of the Itatiaia Alkaline Massif, Southeastern Brazil: New geological insights into a migratory ring Complex', *Brazilian Journal of Geology*, vol. 48, pp. 347-72.

Rosa, P.A.S. 2017, 'Geologia e evolução petrogenética do maciço alcalino de Itatiaia, MG-RJ', Masther´s thesis, Universidade de São Paulo.

Santos, A.C. & Hackspacher, P.C. 2021, 'Meso-Cenozoic Brazilian Offshore Magmatism: Geochemistry, Petrology, and Tectonics', Academic Press, Cambridge.

Schorscher, H.D. & Shea, M.E. 1992, 'The regional geology of the Poços de Caldas alkaline complex: Mineralogy and geochemistry of selected nepheline syenites and phonolites', *Journal of Geochemical Exploration*, vol. 45, pp. 25-51.

Shea, M.E. 1992, 'Isotopic geochemical characterization of selected nepheline syenites and phonolites from the Poços de Caldas alkaline complex, Minas Gerais, Brazil', *Journal of Geochemical Exploration*, vol. 45, pp. 173-214.

Sichel, S.E., Motoki, A., Iwanuch, W., Vargas, T., Aires, J.R., de Melo, D.P., Motoki, K.F., Balmant, A. & Rodrigues, J.G. 2012, 'Cristalização fracionada e assimilação da crosta continental pelos magmas de rochas alcalinas félsicas do estado do Rio de Janeiro', *Anuário do Instituto de Geociências*, vol. 35, no. 2, pp. 84-104.

Sichel, S.E., Motoki, A., Savi, D.C. & Soares, R. 2008, 'Subvolcanic vent-filling welded tuff breccia of Cabo Frio Island, State of Rio de Janeiro, Brazil', *REM: Revista Escola de Minas*, vol. 61, pp. 423-32.

Silva, D.A. 2019, 'Geoquímica e geocronologia (U-Pb e Lu-Hf) das intrusões alcalinas félsicas de Soarinho, Tanguá, Rio Bonito e Tinguá: Implicações sobre as fontes do magmatismo alcalino no Estado do Rio de Janeiro', PhD thesis, Universidade do Estado do Rio de Janeiro.

Silva, D.A., Geraldes, M.C., Vargas, T., Jourdan, F. & Nogueira, C.C. 2015, '$^{40}Ar/^{39}Ar$ age, lithogeochemistry and petrographic studies of the Cretaceous Alkaline Marapicu Intrusion, Rio de Janeiro, Brazil', *Boletim do Museu Paraense Emílio Goeldi-Ciências Naturais*, vol. 10, pp. 399-422.

Silva, D.A., Motoki, A., Santos, A.C., Mendes, J., Jourdan, F., Geraldes, M.C. & Lana, C.C. 2020, 'Multiple processes of geochemical evolution for the alkaline rocks of Rio Bonito intrusive complex, Rio de Janeiro State, Brazil: $^{40}Ar/^{39}Ar$ and U-Pb ages and Lu-Hf isotopes on zircon and constraints on crustal signature', *Geologia USP: Série Científica*, vol. 20, pp. 213-34.

Silva, D.A., Geraldes, M.C., Rodrigues, S.W.O., McMaster, M., Evans, N., Nummer, A.R. & Vargas, T. 2018, '(U-Th)/He Ages from the Fluorite Mineralization of the Tanguá Alkaline Intrusion Idades', *Anuário do Instituto de Geociências – UFRJ*, vol. 41, pp. 14-21.

Silva, D.A., Potratz, G.L. & Geraldes, M.C. 2023, 'Geochemistry and Geochronology (U-Pb and Lu-Hf) of the Soarinho Alkaline Massif (Brazil): Implications on mantle versus crustal signature of syenitic magma', *Minerals*, vol. 13, no. 7, 904.

Silveira, L.S., Dutra, T., Valente, S.C. & Ragatky, D.C. 2005, 'Modelos eruptivos preliminares para o Complexo Vulcânico de Nova Iguaçu, RJ', *Simpósio de Vulcanismo e Ambientes Associados 3*, pp. 333-7.

Smith, P.E., Evensen, N.M., York, D., Szatmari, P., Conceicao, J.C.J., Destro, N., 1999. Getting it on track: Ar-Ar geochronology of alkali intrusions of the Serra do Mar province, Brazil. Eos (Transactions, American Geophysical Union) 80, F1134–F1135.

Smith, P.E., Evensen, N.M., York, D., Szatmari, P. & de Oliveira, D.C. 2001, 'Single-crystal ^{40}Ar-^{39}Ar dating of pyrite: No fool's clock', *Geology*, vol. 29, no. 5, pp. 403-6.

Sonoki, I.K. & Garda, G.M. 1988, 'Idades K-Ar de rochas alcalinas do Brasil Meridional e Paraguai Oriental: compilação e adaptação as novas constantes de decaimento', *Boletim IG–USP: Série Científica*, vol. 19, pp. 63-85.

Takenaka, L.B. 2014, 'Refinamento do método de datação U-Pb *in situ* via LA-Q-ICP-MS: aplicação no Complexo Alcalino Poços de Caldas – MG', Dissertation, Universidade Federal de Ouro Preto.

Thomaz Filho, A., de Cesero, P., Mizusaki, A.M. & Leão, J.G. 2005, 'Hot spot volcanic tracks and their implications for South American plate motion, Campos basin (Rio de Janeiro state), Brazil', *Journal of South American Earth Sciences*, vol. 18, pp. 383-9.

Thompson, R.N., Gibson, S.A., Mitchell, J.G., Dickin, A.P., Leonardos, O.H., Brod, J.A. & Greenwood, J.C. 1998, 'Migrating Cretaceous-Eocene Magmatism in the Serra do Mar Alkaline Province, SE Brazil: Melts from the Deflected Trindade Mantle Plume?', *Journal of Petrology*, vol. 39, pp. 1493-526.

Tsekhmistrenko, M., Sigloch, K., Hosseini, K. & Barruol, G. 2021, 'A tree of Indo-African mantle plumes imaged by seismic tomography', *Nature Geoscience*, vol. 14, no. 8, pp. 612-9.

Ulbrich, H., Demaiffe, D., Vlach, S.R.F. & Ulbrich, M.N.C. 2003, 'Geochemical and Sr, Nd and Pb isotope signatures of phonolites and nepheline syenites from the Poços de Caldas alkaline massif, southeastern Brazil', *South American Symposium of Isotope Geology*, pp. 698-701.

Ulbrich, H., Vlach, S.R.F., Demaiffe, D. & Ulbrich, M.N.C. 2005, 'Mesozoic to Cenozoic Alkaline Magmatism in the Brazilian Plataform', *American Mineralogist*, vol. 92, no. 4, 711.

Ulbrich, H.H.G.J., Vlach, S.R.F., Ulbrich, M.N.C. & Kawashita, K. 2002, 'Penecontemporaneous syenitic-phonolitic and basic-ultrabasic-carbonatitic rocks at the Poços de Caldas Alkaline Massif, SE Brazil: Geologic and geochronologic evidence', *Revista Brasileira de Geociências,* vol. 32, pp. 15-26.

Valença, J.G. 1980, 'Geology, petrography and petrogenesis of some alkaline igneous complexes of Rio de Janeiro State, Brazil', PhD thesis, West Ontario University.

Valença, J., Reis, A.P., Carvalho Filho, C.A., Soares Filho, J.R.S. & Braun, P.V.C.B. 1983, 'Geologia do complexo ígneo alcalino do Morro Redondo (Município de Resende, Estado do Rio de Janeiro)', *Anais da Academia Brasileira de Ciências*, vol. 55, pp. 135-6.

Vlach, S.R.F., Vilalva, F.C.J., Ulbrich, M.N.C., Ulbrich, H.H.G.J. & Vasconcelos, P.M. 2003, 'Phlogopite from carbonatitic veins associated with the Poços de Caldas Alkaline Massif, SE Brazil: Mineralogy and $^{40}Ar/^{39}Ar$ dating by the laser step heating method', *IV South American Symposium on Isotope Geology.*

Wiedenbeck, M.A P.C., Alle, P., Corfu, F.Y., Griffin, W.L., Meier, M., Oberli, F.V., Von Quadt, A., Roddick J.C. & Spiegel, W. 1995, 'Three natural zircon standards for U-Th-Pb, Lu-Hf, trace element and REE analyses', *Geostandards Newsletter*, vol. 19, no. 1, pp. 1-23.

Willbold, M. & Stracke, A. 2010, 'Formation of enriched mantle components by recycling of upper and lower continental crust', *Chemical Geology*, vol. 276, no. 3-4, pp. 188-97.

Author contributions

Marco Aurélio Maia Teodoro: conceptualization; writing-original draft; writing – review and editing; visualization. **Anderson Costa dos Santos:** conceptualization; writing-original draft; writing – review and editing; visualization. **Luiz Carlos Bertolino:** conceptualization; writing – review and editing. **Pedro Augusto da Silva Rosa:** writing – review and editing. **Caio Rodrigues Bezerra:** writing-original draft. **Júlio César Lopes da Silva:** writing-original draft. **Lucas Guimarães Pereira Monteiro:** writing-original draft. **Mariana Bessa Fagundes:** writing-original draft. **Mauro Cesar Geraldes:** formal analysis; methodology. **Leticia Muniz da Costa Cardoso:** formal analysis; methodology. **Fred Jourdan:** formal analysis; methodology.

Conflict of interest

The authors declare no conflict of interest.

Data availability statement

All data included in this study are publicly available in the literature.

Funding information

CNPq (ProTrindade Program) [Process number. 557146/2009-7]; MCT/CNPq project [number 26/2009]; and FAPERJ [Entidades Estaduais 2018 number 210.297/2018; APQ1 2019 number 210.179/2019; JCNE 2022 number 201.469/2022].

Editor-in-chief

Dr. Claudine Dereczynski

Associate Editor

Dr. Gustavo Luiz Campos Pires

How to cite:

Teodoro, M.A.M., Santos, A.C., Bertolino, L.C., Rosa, P.A.S., Bezerra, C.R., Monteiro, L.G.P., Silva, J.C.L., Fagundes, M.B., Geraldes, M.C., Cardoso, L.M.C. & Jourdan, F. 2025, 'Poços de Caldas – Cabo Frio Alignment: a Petrochronological Review of an Unconventional Plume Model', Anuário do Instituto de Geociências, vol. 48, e65281, DOI: 10.11137/1982-3908_2024_48_65281.